Accepted Manuscript

Journal of the Geological Society

Mid-crustal reactivation processes linked to frictional melting and deep void development during seismogenic slip: examples from the Lewisian Complex, NW Scotland

K. Hardman, R. E. Holdsworth, L. Scott, E. Dempsey & K. J. W. McCaffrey

DOI: https://doi.org/10.1144/jgs2022-037

To access the most recent version of this article, please click the DOI URL in the line above. When citing this article please include the above DOI.

Received 11 March 2022
Revised 6 October 2022
Accepted 19 November 2022

Mid-crustal reactivation processes linked to frictional melting and deep void development during seismogenic slip: examples from the Lewisian Complex, NW Scotland

Hardman, K.[1], Holdsworth, R. E.[1,2], Scott, L. [1], Dempsey, E.[3], McCaffrey, K. J. W.[1,2]

1 Department of Earth Sciences, Durham University, DH1 3LE, UK
2 Geospatial Research Ltd, Durham DH1 4EL, UK
3 Department of Geography, Geology and Environment, University of Hull, HU6 7RX, UK

ABSTRACT

Exhumed examples of ancient fault voids formed during seismic slip at depths > 10 km are well preserved in the Assynt Terrane of the Lewisian Complex, NW Scotland. They are interpreted to have formed during regional Mesoproterozoic (ca 1.55 Ga; '*Assyntian*') strike-slip faulting. Deformation is characterised by sinistral reactivation of pre-existing NW-SE trending features including intrusive contacts of (ca 2.4 Ga) mafic dykes and Paleoproterozoic ductile shear zone fabrics (ca 1.75 Ga). Reactivation occurred at palaeodepths of 10-15km, where frictional-viscous deformation synchronous with co-seismic frictional melting led to cycles of mm to dm-scale cavity dilation and collapse. Although individual melt-generating slip surfaces may have become rapidly welded, faulting was able to repeatedly localise along adjacent pre-existing planar anisotropies favourably oriented for slip leading to the creation of a mesh of foliation-parallel melt generation surfaces linked by foliation-perpendicular dilational voids. The latter features are filled by chaotic clast-supported wall rock collapse breccias, localised injected frictional melts and hydrothermal mineralization. The fills act as natural props, holding cavities open and preserving them as long-term, pipe-like fluid flow conduits. These exhumed features

are likely to be typical of multi-rupture seismogenic fault systems formed by direct reactivation of pre-existing basement structures.

Introduction

A number of recent studies have emphasized the importance of near-surface dilatant fissure and void formation in areas where (mainly normal) faulting occurs in relatively strong, low permeability rocks such as basalts, crystalline basement rocks and carbonates (e.g. Holland *et al.* 2006, 2011; van Gent *et al.* 2010; Walker *et al.* 2011; Weismüller *et al.* 2019; Hardman *et al.* 2020; Holdsworth *et al.* 2020a). Experimental testing and geomechanical modelling have shown that open voids can be stable to great depths, even in the absence of overpressure (e.g. Davis *et al*. 2017); for example, open cavities are known to exist below 8 km depth in several ultradeep hydrocarbon basins (e.g Tarim Basin, China, Ukar *et al.* 2020). Such subterranean cavities have the potential to significantly influence the flow and storage of subsurface water, hydrothermal mineralizing fluids, magma, and hydrocarbons. Therefore, research into fault-related void formation is of potential significance in the assessment of worldwide geological resources, geothermal reservoirs and geohazards.

Three related areas of current uncertainty are concerned with: i) how the development of these dilational phenomena may be related to seismogenic slip processes along brittle fault systems (e.g. Holdsworth *et al*. 2019); ii) understanding the depth range over which such dilational features may form along active crustal fault zones (e.g. Holland *et al.* 2011); and iii) understanding the preservation potential and mechanisms of deep void formation and filling. The well exposed and accessible basement gneisses of the Neoarchaean Lewisian Gneiss Complex in NW

Scotland (Fig. 1) are an ideal location to explore some of these uncertainties. In these rocks, an array of geological processes can be examined that have occurred across a broad range of depths during a long history of deformation that spans close to three billion years. A series of distinct tectonic events are recognised, each associated with different P-T conditions broadly reflecting the apparent relative progressive exhumation of these rocks from the lower crust at ca 2.8 Ga to the surface by ca 1.2 Ga (Park 2005; Wheeler *et al.* 2010; MacDonald *et al.* 2015; Holdsworth *et al.* 2020b). The structures include very well-preserved examples of faults formed close to the frictional-viscous transition which are widely associated with the development of pseudotachylytes (friction melts) (e.g. Sibson 1975; Beacom *et al*. 2001; Imber *et al*. 2001; Sibson & Toy 2006).

In this paper, we present field and microscopic observations, supported by stress inversion and fracture topology analyses from exceptionally well-exposed ancient seismogenic fault zones in Lewisian rocks from the Achmelvich area (Fig. 1). We show that these faults are particularly well developed in areas where pre-existing, steeply dipping to sub-vertical geological structures, such as foliations and dyke contacts have been reactivated, and that in some cases, large (up to dm-scale) dilational cavities were formed directly associated with ancient seismogenic faulting events. Whilst active cavity development may be transient at such great depths (ca 10-15 km), we show that geological processes can lead to natural (or self-) propping of partially open dilation sites (cf Holdsworth *et al.* 2019, Cheng and Milsch 2021) that can then be preserved over long geological timescales. This has important potential implications for the fluid transport and storage properties, and the economic potential of crystalline basement terrains worldwide.

Geological Setting

The Precambrian rocks of the Lewisian Gneiss Complex, NW Scotland form a fragment of the continental basement of Laurentia that lies to the west of the Palaeozoic Caledonian orogenic belt (Fig. 1). The rocks preserve evidence for a superimposed sequence of crustal-scale geological events that occurred from the Neoarchaean to the present day (Sutton & Watson 1951; Park 1970; Park *et al.* 1994; Wheeler *et al.* 2010; McCaffrey *et al.* 2020).

The Assynt Terrane (Fig. 1a, b) forms the central part of the Lewisian Gneiss Complex in mainland NW Scotland. It is mostly composed of grey, banded, tonalite–trondhjemite–granodioritic (TTG) gneisses which are locally highly heterogeneous in composition, and include distinct mafic-ultramafic units (e.g., Sheraton *et al.* 1973; Guice *et al.* 2020). The TTG gneisses are thought to be derived from igneous plutons which were intruded into the crust at ca 2.85-3.03 Ga (high precision U-Pb and Sm-Nd geochronology; Whitehouse 1989; Park 2005; Whitehouse & Kemp 2010, Whitehouse *et al.* 2022). These gneisses have subsequently undergone a series of Neoarchaean to Mesoproterozoic deformation episodes prior to their final exhumation at the surface during the deposition of the overlying Stoer Group sediments in the Neoproterozoic (ca 1.2 Ga) (Beacom *et al.* 2001; Holdsworth *et al.* 2020b).

Following their initial emplacement as plutons, the basement rocks first experienced deformation and granulite facies metamorphism (~1000°C, 11-15kbar, ca 30 km depth) during the so-called *Badcallian* event(s) the timing of which is incompletely resolved (Wheeler *et al.* 2010; Whitehouse & Kemp 2010). Current age constraints suggest either a more widely favoured age of ca 2.76 Ga (e.g; Corfu *et al.* 1994; Zhu *et al.* 1997; MacDonald *et al.* 2015), and/or a younger age of ca 2.48–

2.49 Ga (e.g., Friend & Kinny 1995; Kinny *et al.* 1999). In the central part of the Assynt Terrane, the generally flat-lying Badcallian structures are refolded and cross-cut by a steeply-dipping, kilometre-scale NW-SE-trending zone of high-strain ductile deformation known as the Canisp Shear Zone (CSZ; Attfield 1987; Park & Tarney 1987; Fig. 1c). This dextral transpressional shear zone is thought to have developed initially during *Inverian* deformation and amphibolite-facies retrogression which affected substantial parts of the Assynt Terrane (e.g. Evans & Lambert 1974; Attfield 1987). Mineral assemblages (Beach 1976) and deformation textures (Jensen 1984) suggest that significant exhumation had occurred since the Badcallian to depths in the range 15-25km (520-600^{o}C). The absolute age of this event is also somewhat uncertain, but a majority of studies favour an age of ca 2.4 Ga (e.g., Corfu *et al.* 1994; Love *et al.* 2004; Goodenough *et al.* 2013).

The Badcallian and Inverian structures are cross-cut by a regionally extensive set of NW-SE trending mafic and ultramafic intrusions known as the *Scourie dyke suite* (Fig. 1b). They are thought to have been emplaced under amphibolite facies temperatures and pressures due to the autochthonous alteration of igneous pyroxenes to hornblende along the chilled margins of undeformed dykes (Tarney, 1963; Scott 2019). Individual intrusions range in thickness from a few millimetres to several tens of metres and were intruded as two suites of differing age: a dominant ca 2.42-2.38 Ga set and a more minor group at ca 2.0 Ga (Rb-Sr whole rock and U-Pb geochronology; Chapman 1979; Heaman & Tarney 1989; Davies & Heaman 2014).

The dykes and older structures in the host rock gneisses of the Assynt Terrane are cross-cut by a regional set of *quartz-pyrite veins*, the emplacement of which has been dated using Re-Os geochronology at ca 2.26 Ga (Vernon *et al.*

2014). These veins, and all older structures, are then heterogeneously overprinted by younger deformation with widespread retrogression of the TTG gneisses under lower amphibolite to upper greenschist facies metamorphic conditions (e.g., Sutton & Watson 1951; Attfield 1987; Beacom *et al.* 2001). This regionally recognised *Laxfordian* event begins with a series of magmatic and high grade (upper amphibolite to locally granulite facies) events ca 1.9–1.87 Ga, followed by a protracted orogenic episode lasting from 1.79 to 1.66 Ga (see Park 2005; Goodenough *et al.* 2013). In the Assynt Terrane, the effects of Laxfordian reworking during dextral transpression are highly localised, being largely restricted to a 1 km wide zone at the centre of the Canisp Shear Zone (CSZ) and other, smaller local shear zones (e.g. Stoer shear zone), as well as along the margins of the Scourie dykes (Attfield 1987; Fig. 1c, 2a). The phyllosilicate-rich mineralogy and deformation textures associated with dextral Laxfordian shear both in the central part of the CSZ and along dyke margins outside of the CSZ are consistent with lowermost amphibolite to greenschist facies metamorphic conditions just below the frictional-viscous transition (~450-500^{o}C, ca 15 km depth; Beach 1976; Jensen 1984; Attfield 1987; Chattopadhyay *et al.* 2010; Wilson *et al.* 2011; MacDonald *et al.* 2017).

In both the Assynt and Gruinard terrane to the southwest (Fig. 1a), a younger set of strike-slip brittle-ductile shear zones, brittle faults and localised folds is recognised developed sub-parallel (NW-SE) to the pre-existing high-strain Laxfordian and Inverian fabrics, and the margins of many Scourie dykes (Lei Shihe & Park 1993; Beacom *et al.* 2001; Holdsworth *et al.* 2020b) These structures are widely associated with the development of pseudotachylytes formed due to rapid frictional melting during earthquake slip events along local fault zones. Rhenium-Osmium geochronology of localized syn-tectonic copper-iron hydrothermal

mineralization near Loch Assynt (Fig. 1c; Holdsworth *et al.* 2020b) yielded an age of ca 1.55 Ga for this faulting episode. Related epidote-quartz-chlorite mineralization is ubiquitous and, together with the typical depth range of most pseudotachylytes worldwide (Sibson & Toy 2006; Fagereng & Toy 2011), suggests that these faults likely formed under lower greenschist facies conditions (ca 300-450^{o}C) at depths of 10-15 km, close to the frictional-viscous transition assuming a standard continental geothermal gradient of 30°C km^{-1}. The associated NW-SE sinistral faults are kinematically distinct from the regional dextral displacements associated with significantly older Laxfordian deformation. Therefore Holdsworth *et al.* (2020b) have proposed that these c. 1.55 Ga structures are termed *'Assyntian'* rather than the previously used term 'Late Laxfordian'.

The Assyntian structures are post-dated by deposition of the unmetamorphosed and little-deformed ca 1.2 Ga Stoer Group sedimentary sequence (Holdsworth *et al.* 2020b; Killingback *et al.* 2020). This demonstrates that the presently exposed parts of the Lewisian Complex within the Assynt Terrane had been exhumed to the surface by that time. Regionally, both the Stoer Group and the wider Lewisian Complex are in turn unconformably overlain by younger Torridonian sequences thought to have been deposited no earlier than 1.04 Ga (Park *et al.* 1994).

The present study focuses on exceptionally well exposed Assyntian fault zones found near to the present-day coastline in the northern parts of Enard Bay in the Achmelvich-Stoer region (Figs 1c, 2a).

Field and laboratory methods

Fieldwork, sampling and petrography

Deformation structures affecting Lewisian gneisses and Scourie dykes were studied in the field using selected coastal outcrops from Lochinver to Clachtoll, and inland close to the north shore of Loch Assynt (Fig. 1c). The relative ages of country rock fabrics, igneous intrusions, mineral veins and fault rocks were ascertained from observed cross-cutting relationships. Structural geometries and kinematic relationships were recorded through collection of orientation and displacement vector data. Structural data were primarily collected in-field using compass-clinometers supplemented with orientation data derived from interpreted lineaments from orthorectified (planimetrically correct) virtual outcrop models and aerial imagery. Shear zone and later faulting kinematics were determined using ductile (asymmetric shear zone fabrics, porphyroclasts and S-C-C' fabrics; e.g. Passchier & Trouw 2005) and brittle (offsets of piercing points, en-echelon veins and slickenline steps, e.g. Petit 1987) shear sense criteria. A representative sample set of orientated hand specimens were collected for thin sectioning and transmitted light microscopy was used to study petrography, microstructures, and overprinting relationships.

Quantitative analysis of brittle structures

Palaeostress inversions are a series of numerical and stereographic projection techniques that allow an approximation of the stress conditions that existed for a given set of coeval faults and fractures at the time of their formation using recorded fault vector data (i.e. slickenlines) (Angelier 1991). These techniques broadly assume that the slip vector data recorded in the field lie parallel to the shear component of the resolved stress tensor (Wallace 1951; Bott 1959). This assumption is reasonable if fault displacements are limited (finite strains low, with little rotation of fault blocks), a condition met by the small-displacement structures considered here.

An analysis was undertaken on high-confidence slickenline data measured from 50 fault planes assigned to the Assyntian reactivation event across multiple outcrops in the Canisp Shear Zone (CSZ) and adjacent areas. Data were only included in the sample set if there was a clear indication of shear sense and were first corrected for later exhumation-related regional tilting (24^{o} clockwise, around an axis of 00-007 – derived from palaeodips of overlying Stoer Group strata) prior to inversion. Due to the sub-vertical nature of the fault planes, the lineation data were recorded in the field as pitches/rakes on the fault plane to improve accuracy of data collection. The Improved Right Dihedron method based on Angelier & Mechler (1977) was applied using WinTensor software (Delvaux & Sperner 2003).

A *slip tendency analysis* was also carried out for the Assyntian faults as they are almost exclusively reactivations of pre-existing ductile foliations and dyke margins (see Morris *et al.* 1996; Lisle & Srivastava 2004; Dempsey *et al.* 2014 for background and rationale). The normalised slip tendency analysis defines the propensity of a measured plane to slip under the resolved stress field with an imposed (i.e. assumed) frictional coefficient (Morris *et al.* 1996; Lisle & Srivastava 2004). This analysis is presented as a ratio, where critically stressed fault orientations have a value close to 1 and non-stressed faults have a value close to 0.

Fracture topology is a network characterisation technique that simplifies a 2D fault or fracture network into discrete branches and nodes (Sanderson & Nixon 2015). It is used to define both the geometrical features and relationships between elements of a network and is a particularly useful way to describe fracture interconnectivity and therefore potential fluid transport properties. The ratios between different types of nodes (I-T or T-X; Isolated, Terminating, Cross-cutting), and branches can be used to determine the relative connectivity and spatial

characteristics of the studied fracture network. In particular N_B/N_L ratios – the ratio of the number of fractures branches (fault trace between two nodes) versus the number of fault lengths (total faults between two tips or sampling boundaries) is used as a proxy for connectivity for a given fault network (Sanderson & Nixon 2015). In this study, fracture topology was calculated by hand from 2D planar images taken from a variety of scales, using orthorectified, planimetrically-correct fracture trace maps, generated from 3D virtual outcrop models of key localities (yellow boxes in Fig. 2a). The 3D models were built using structure-from-motion photogrammetry from photos taken from a drone in Agisoft's Photoscan software, now called Metashape (e.g. Tavani *et al.* 2014). The generated models have sizes of 10000^2 pixels with an effective viewing resolution of a few millimetres. Models were then interpreted manually using vector graphics software (Adobe Illustrator) at fixed zoom intervals using a single fixed resolution monitor to reduce bias/drift in interpretation density. This was necessary due to the exceptionally large number of fractures visible ($>10^5$ per model).

Field and cross-cutting relationships

The earliest features preserved in the gneisses of the Achmelvich-Stoer region are best observed on the tidally-exposed outcrops either side of Achmelvich Beach (NC 0549 2491, and NC 0568 2546) (Figs 1, 2a, b). Shallowly NW- to N-dipping compositional layers (ranging from 1mm-100cm thick) comprise alternating bands of mafic and leucocratic granodioritic to dioritic orthogneiss (Fig. 2b).

The amphibolite facies Inverian event is represented within the study area by the steepening of the Badcallian foliation to form the Lochinver monocline (Evans and Lambert 1974) (Figs 2a, c) and the development of the 1.5-2.5 km wide Canisp

Shear Zone (CSZ) and its associated structures (Attfield 1987). This is a zone of intense NW-SE sub-vertical gneissic foliation (1-15cm thick), tight minor folds, and steeply-obliquely plunging mineral lineations (Fig. 2c; Chattopadhyay *et al*. 2010).

The metadoleritic Scourie dykes cross-cut Badcallian and Inverian structures varying in width from centimetres to tens of metres and may extend laterally for many kilometres along strike (Figs 1b, 2a, 3a). North of Achmelvich Beach (NC 0565 2507), a xenolith of foliated gneiss (40x170 cm) is encapsulated within an 30 m wide metadolerite dyke preserving the older Badcallian and Inverian fabrics within the gneiss (Fig. 3a, b). The original cross-cutting nature of the dykes is commonly partially to totally obscured by the development of later shear zones and faults that localize along, and reactivate the dyke margins during Laxfordian and younger deformations (Wilson *et al.* 2011).

A central part of the CSZ ~0.5 km wide is dominated by an overprinting Laxfordian ductile deformation (Fig. 2a), comprising sub-vertical high-intensity schistose fabrics (Figs 2d). Scourie dykes here are transformed into amphibolites sheared into near concordance with the surrounding foliation in the gneisses (Fig. 2d, 3c, d; e.g. NC 0549 2491, and NC 0568 2546; Sheraton *et al.* 1973; Attfield 1987; Scott 2019). The subvertical NW-SE foliation is associated with shallowly-plunging mineral lineations and widespread dextral shear criteria (Figs 2a, d, 3e) (Attfield 1987; Beacom *et al.* 2001; Wilson *et al.* 2011). The foliation locally anastomoses and coalesces around tight to isoclinal intrafolial (sheath) folds (Chattopadhyay *et al.* 2010) which act as local regions of lower strain where refolded Inverian or Badcallian folds and fabrics are locally preserved, together with cross-cutting amphibolites derived from otherwise transposed Scourie dykes (e.g. as seen on the coast at Port Alltan Na Bradhan, e.g. NC 0479 2627).

Dyke margins outwith of the CSZ also feature <20cm wide developments of NW-SE schistose Laxfordian mylonites, both in the metadolerite and adjacent granitic gneiss (Figs 3c, d; NC 0549 2492, NC 0568 2546). These schistose micaceous fabrics feature shallowly plunging mineral lineations, S-C fabrics (Fig 3f), and asymmetric bending of foliations from regions of high strain to low strain that consistently demonstrate ductile dextral shear (Figs 3d, e).

Steeply-dipping to subvertical NW-SE brittle-ductile structures related to the Assyntian (previously 'late-Laxfordian') event localize along - and therefore reactivate - earlier ductile Laxfordian fabrics in the central part of the CSZ (Fig. 4a-c and along Scourie dyke margins (Fig. 3c, 4d-f; Beacom *et al.* 2001; Holdsworth *et al.* 2020b). In the central CSZ, fault surfaces running parallel, or at low angles to the pre-existing schistose foliation preserve shallowly plunging slickenlines (Fig. 4g). Sinistral senses of shear are indicated by local offsets of markers, the development of shear band fabrics in phyllosilicate-rich horizons, the presence of dilational jogs, and by the development of mm to cm-scale, steeply-plunging, S-shaped folds (Fig. 4h). At the dyke margins, dextral ductile mylonites are overprinted by low offset (<30cm) brittle faults that host brecciated schistose material and low-angle sickenfibres that show sinistral offsets (Fig. 4d-f). These structures are widely associated with quartz-epidote-chlorite-hematite mineralization, local occurrences of ultramylonite and frictional melts (pseudotachylytes, e.g. Fig. 4f), all of which are consistent with their development under lower greenschist facies metamorphic conditions close to, or just above the frictional-viscous transition (c. 300-450^{o}C; 10-15km depth).

The youngest features observed locally lie close (<5m) to the basal breccia of the Clachtoll Formation, the oldest part of the unconformably overlying Stoer Group..

At NC 0416 2654, tensile fractures are filled with Stoer Group sediment and form a small network, with a sub-horizontal <10cm wide cavity, cutting two E-W-trending sub-vertical foliation-parallel fractures <6cm wide (Fig. 5). The fracture cavities are evenly filled with three separate sedimentary packages subtly distinguished by differences in grain size and colour. These highly localised sediment-filled fractures are thought to have formed when clastic material was washed into local open fissures formed at the surface ca 1.2 Ga ago (see also the features overlying the megaclast feature described at Clachtoll by Killingback *et al.* 2021).

The geological characteristics of Assyntian reactivation

We focus first on the development of frictional-viscous Assyntian structures in the central part of the CSZ at Achmelvich as this represents the region where these structures are most intensely developed (e.g. Beacom *et al.* 2001; Wilson *et al.* 2011). We then briefly compare and contrast these features with equivalent-age structures that are locally developed along reactivated dyke margins outwith of the CSZ in the Achmelvich and Loch Assynt areas (Fig. 1c).

Central Canisp Shear Zone

Mesoscale features: The Assyntian structures of the Canisp Shear Zone are dominated by two sets of mutually cross-cutting faults and fractures (Fig. 6a). A NW-SE trending set of sinistral strike slip faults - formed sub-parallel, or at low angles to the pre-existing sub-vertical ductile foliation - and a dextral-extensional fault set trending NNE-SSW sub-perpendicular to the foliation (Figs 4b, c, 6a, b). Given their mutually cross-cutting behaviour, these faults are interpreted to be broadly coeval; they are, however, geologically quite distinct from one another. In all cases,

however, the Lewisian host rocks adjacent to these fault sets (<2cm from a fracture surface) are pervasively and distinctively stained dark red/brown due to the percolation of iron-rich hematitic fluids throughout the fault network (e.g. Fig. 6b).

The sinistral NW-SE foliation-parallel faults are shear fractures with multi-metre displacements – as measured from offset markers where preserved. Hundreds – possibly thousands - of these faults are developed throughout the central part of the CSZ with typical damage zones 2-6 cm wide (Beacom et al. 2001). Many, but not all, of these faults are locally associated with narrow continuous bands of pseudotachylyte (0.5-5cm thick) developed along very long fault planes (10s-100s metres), with the rare presence of small sinistrally-verging folds (Figs 4b, h, 6c, d). Locally-preserved slickenlines (Fig. 4g) are consistent with both sinistral and reverse slip offsets.

The NNE-SSW foliation-perpendicular faults rarely show shear offsets greater than a few centimetres. Where present, these demonstrate a minor dextral component to the slip (Fig. 6a). They are much wider in aperture than the foliation-parallel structures (up to tens of centimetres wide) with metre-wide damage zones defined by micro-fracture arrays and complex shapes (e.g. Fig. 6b, e, f). These foliation-perpendicular faults have much shorter lengths (typically 0.5 to 2m) and are commonly bounded at their ends by foliation-parallel faults (Fig. 6f). A small number of foliation-perpendicular faults (e.g. at NC 0486 2621) have a longer trace length (e.g. up to 50m) with greater shear offsets (up to a few metres) and appear to have formed from the linking together of several sets of foliation-perpendicular structures.

Microscale features: The foliation-parallel faults are associated with thin continuous veins of frictional melt – pseudotachylyte (Fig. 4c, 7a). In thin section under high

magnification, the pseudotachylytes show characteristic dendritic to spherulitic silica microcrystallites suspended in an amorphous dark matrix (Fig. 7b). This microstructure is consistent with a fast cooling rate (Kirkpatrick & Rowe 2013). Many melt-bearing, foliation-parallel shear fractures also display characteristic v-shaped injections or 'wing-crack fills' that are widely associated with pseudotachylyte developments globally (e.g. Fig. 7a, c and f; Di Toro *et al.* 2006; Rowe *et al.* 2018; Campbell *et al.* 2020). In some veins, clasts of older pseudotachylyte are preserved 'floating' in a matrix of younger frictional melt (Fig. 7g) and features interpreted to be injections are seen in outcrops locally cross-cutting one another suggesting multiple phases of local seismicity and associated melting along discrete faults.

The foliation-parallel friction melts are locally exceptionally well exposed both in cross section (Fig. 7c) and along-plane and may display complex flow patterns (Fig. 7d). These flow striae are defined in outcrop by ridges and textures on the melt surface and by grain size variation and clast frequency in thin section. The flow patterns show no clear orientation relationship to slickenlines suggesting that they record the local migration of melt possibly driven by differences in pressure during seismogenic slip (Fig. 7d, e; Sibson 1975).

The foliation-perpendicular fractures show a highly diverse range of associated fills and are markedly dilational in character where bounded blocks are variably tilted and offset forming irregular 'ladder fracture' arrays (e.g. Fig. 6e, f). A range of heavily iron-stained breccias are developed with angular clasts of wall rock and variable volumes of finer grained matrix material (e.g. Figs 6, e, f, 8a, b). Clast contents vary from 30-90% by volume, with the great majority being greater than 70%; thus, most are strongly clast supported. Following the terminology of Woodcock & Mort (2008), these fracture fills range from crackle breccias defined by

approximately conjugate sets of shear fractures (Fig. 6b, the ‘ladder fractures’ of Beacom *et al.* 1999) through to completely chaotic breccia made up of disaggregated collections of angular wall rock clasts bounded by relatively planar fractures on one or both sides (Fig. 6e, f, 8a). The angular clasts range from 1 to 10s of cm along their longest axis and show no sorting, preferred orientation or any uniform rotation direction. A variety of matrix fills are present (see below), but are commonly heavily iron-stained.

In a few localities, the foliation-perpendicular fractures also contain green epidote-cemented porous cataclasites and micro-breccias, particularly around Alltan Na Bradhan (NC 0486 2621) (Fig. 8b). These have lower clast contents (typically <30%) and appear to have formed where a greater degree of shear offset and attrition of clasts has occurred. Such less widespread, foliation-perpendicular faults have metre-scale dextral offsets and complex anastomosing and coalescing geometries with lengths of several tens to hundreds of metres.

Matrix fills comprise mineral cements and fine clasts of wall rock material. The mineralogy of the mnieraslization and fault rock cements is notably diverse (Figs 8b-e). Limited cross-cutting relationships suggest that an earlier phase of cementation led to the development of hematite-cemented clasts of wall rock (Figs 8d). A second phase of more complex epidote, pyrite, quartz, chalcedony, chlorite and prehnite mineralisation is best seen in reactivated fault rocks, lining exposed fault walls (Figs 8c, e-g). Regionally, epidote is always associated with Assyntian structures and, in the Loch Assynt locality, Holdsworth *et al.* (2020b) have demonstrated that it is co-genetic with the sulphides that yielded the ca 1.55 Ga age using Re-Os geochronology. The youngest mineral fills are localized occurrences of calcite and zeolite veins. Despite the textural variation between the brecciated fault voids fills,

they are all highly porous, and preserve significant vuggy cavities from a micro to mesoscale (<1mm up to 10cm in diameter) (Fig. 8a, c).

A key feature seen in a number of foliation-parallel and foliation-perpendicular intersections is the presence of pseudotachylyte injections into abutting dilatant-fractures and crackle breccias, akin to examples reported by Rowe *et al.* (2018). This shows that whilst the two sets of fractures are very different in their geological character, both are contemporaneous with, and therefore related to, the development of the same frictional melts during seismogenic slip. When viewed in thin section, the injected pseudotachylytes show vesicles, features that are only seen in these intersection points (Fig. 7h). These are thought to represent bubbles that formed from the near instantaneous depressurisation of the melt following injection (e.g. Chernov *et al.* 2014).

Scourie dyke margins

Many, but not all, exposed NW-SE-trending steeply-dipping dyke margins show some evidence of reactivation during either Laxfordian and/or Assyntian deformation. Good examples of ductile dextral Laxfordian reactivation are preserved along the southern contact of the dyke exposed at NC 0549 2491 and on the northern contact of the dyke at NC 0568 2546 (Scott 2019), on the southern and northern sides of Achmelvich beach, respectively (Fig. 3a). Brittle fractures associated with both of these dykes (interpreted to be Assyntian) form two main sets: NW-SE trending faults trending sub-parallel to dyke margins and a set of NE-SW trending tensile fractures. These sets are mutually cross-cutting and abutting and are therefore interpreted to be coeval. The dyke margin-parallel shears host brecciated schistose material, and 1-5 cm-thick bands of cataclasite associated with <2.5 cm-thick pseudotachylytes,

and a variety of different hydrothermal minerals (Figs 4b-f). The cataclasites and breccia contain significant volumes of chlorite (15%), quartz (10%), and hornblende (15%) set in a quartzofeldspathic microcrystalline matrix (<10μm grains). These brittle fabrics show offsets of gneissose banding, S-C fabrics, Riedel shears, kink-banding, and shallowly-plunging slickenlines all of which indicate sinistral strike-slip (Figs 4d-f). Adjacent to the dyke at NC 0549 2491, tensile fractures within the gneiss trend NE-SW and are locally injected by <1cm wide bands of frictional melt that originate from the prominent NW-SE fault that forms the northern margin of the dyke. Cross cutting the pseudotachylytes and the dyke are pale-coloured zeolite veins trending ENE-WSW and in NE-SW trending pull-apart features. The faulted dyke margin is prominently stained red-brown colour by hematite which extends along fractures up to 3m from the contact into the surrounding wall rock gneiss.

At Loch Assynt, 15km east of Achmelvich, two subvertical dykes (40m and 10m wide) sharply cross-cut the pre-existing gneissic foliation, and are in turn cut by a regional suite of (ca 2.26 Ga) quartz-pyrite veins (Vernon *et al.* 2014) . Brittle reactivation of dyke margins by sinistral faults with associated Riedel shears is observed, marked locally by the development of 1-5cm thick bands of dark foliated ultramylonites (Figs 4f; NC 2104 2519; Holdsworth *et al.* 2020b). These ultra-fine-grained (0.1-0.5mm) fault rocks feature S-C banding consistent with sinistral shear and are closely associated with narrow bands of frictional melt and quartz-epidote veining (c.1mm wide) (Fig. 4f). Millimetre-scale dilational jogs observed in the quartz-epidote veins both within the dyke and at the margins consistently indicate sinistral shear, whilst exposed vein margins exhibit sinistrally-stepping quartz-epidote slickenfibres (Holdsworth *et al.* 2020b).

Palaeostress inversion analysis

The principal stress axes derived from the stress inversion analysis indicate E-W compression and N-S extension. This is true for all data collected at Achmelvich (Fig. 9a) and also for a subset of that data from the exceptional set of exposures at Cathair Dubh (Fig. 9b, location shown on Fig 2a). The deduced stress axis orientations are consistent with strike-slip faulting and give almost identical results to the stress inversion analysis carried out on Assyntian structures at Loch Assynt (see Holdsworth et al. 2020b, their figure 9). The results of the slip tendency analysis show that steeply-dipping, ESE-WNW planes oriented parallel or at low angles to the foliation are most favourable for slip in the regionally determined stress field (Fig. 9c); this is consistent with the field observations and the development of the foliation-parallel shear fracture set. The Assyntian fractures seen within the collected kinematic data (see Fig. 6a, 9a-c), including the foliation-perpendicular dextral faults and tensile sets, conform broadly to the fracture criteria defined by Petit (1987). This suggests that the dextral foliation-perpendicular (R'), tensile (T), and more E-W oriented sinistral faults (R) formed during sinistral shear along principal foliation-parallel faults (Y) (Fig 9d, e).

Fracture Topology

In order to assess the fracture connectivity, fracture topology analyses were carried out using orthorectified fracture trace maps, generated from 3D virtual outcrop models of key well-exposed localities (Fig. 10). The results of these analyses showed that at all scales studied, the N_B/N_L ratios were consistently >2.0 indicating a highly connected network. In addition, the results show a dominance of "T" nodes over "I" or "X" and C-C type branches over I-C or I-I (Fig. 10, Table 1; see Sanderson

& Nixon 2015 for further details). This indicates that the fracture and fault systems here are very well-connected at all scales. The high fracture intensity recorded within the Assyntian fault zones (locally up to $40m^{-1}$, see also Beacom *et al.* 2001), combined with the results of the topological analysis show that the basement here is potentially exceptionally permeable to geological fluids, particularly in a sub-vertical direction parallel to the dominant fracture intersection orientation (Figs. 6a, 9e).

Discussion

Summary of field relationships

The ca 1.55 Ga Assyntian deformation in the Achmelvich-Loch Assynt area is characterised by the sinistral reactivation of steeply-dipping, pre-existing NW-SE trending features including intrusive contacts of mafic dykes and Paleoproterozoic ductile shear zone fabrics. Reactivation occurred at palaeodepths interpreted to be in the range 10-15 km based on palaeotemperature estimates. Faulting localises along pre-existing planar anisotropies favourably oriented for left-lateral slip leading to the development of multiple foliation-parallel melt generation surfaces. In the phyllosilicate-rich CSZ, hundreds of these sub-parallel slip surfaces are linked by foliation-perpendicular (NE-SW) dilational voids and extensional/transtensional fractures (Fig. 11a). The latter features are filled by chaotic, clast-supported wall rock collapse breccias, localised injected frictional melts and a range of hydrothermal mineral fills.

The relative ages of the foliation-parallel and -perpendicular fracture sets

The outcrops at Achmelvich-Clachtoll have previously been described by Beacom *et al.* (1999, 2001). These authors attributed the sinistral foliation-and dyke-parallel

faulting to Assyntian (formerly “Late-Laxfordian”) deformation. However, these authors suggested that the breccia-filled, foliation-perpendicular ‘ladder fractures’ within the CSZ were formed in the near-surface during transtensional faulting synchronous with deposition of the overlying Stoer Group. We disagree with this interpretation for three reasons.

1. Foliation-perpendicular fractures are observed to be both cross-cut by, and to cross-cut the foliation-parallel faults. This relationship was noted by Beacom *et al.* (1999) who suggested that some foliation-parallel faults were reactivated as transfer faults during Stoer Group-age rifting. Careful re-examination of all the outcrops suggests, however, that the mutual cross-cutting relationships are too ubiquitous to be interpreted in this way and that they can only form through episodic and contemporaneous deformation within a regionally consistent tectonic stress field, which the palaeostress analysis suggests is plausible.
2. Frictional melts and veins which originate within the foliation-parallel faults are seen at several localities to be injected into dilatant foliation-perpendicular fractures (e.g. at NC 0535 2576, NC 0576 2554, NC 0419 2659). This can only occur if the latter are present and open(ing) during melt-generating slip events along the foliation-parallel faults. This observation was not made by Beacom *et al*. (1999) who correlated the foliation-perpendicular fractures with sediment filled fractures seen close to the base of the Stoer Group at Clachtoll. We have been unable to find <u>any</u> sedimentary material in regions located more than a few metres from the Stoer Group, with the exception of a single breccia fill near an exposed hilltop at NC 0534 2495. Here a small 3-4cm wide dilatant fracture is filled with a pale grey-tan sediment and breccia

(Fig. 5b). This ESE-WNW fracture abuts a larger NNE-SSW oriented fault, seen clearly in satellite imagery cutting the headland south of Achmelvich Bay. This sediment filled fracture is interpreted to be a later exhumation-related feature associated with rifting and deposition of the Stoer Group in the near-surface. Notably, the sediment fill here lacks haematite staining and is oriented almost perpendicular to the Assyntian breccia-filled faults.

3. The pervasive fracture- and microfracture-hosted iron-staining of the gneisses surrounding both the foliation-perpendicular and foliation-parallel faults suggests that the slip on both sets of faults was closely associated with the flux of iron-rich fluids bearing in mind that this mineralization is texturally the earliest stage. This staining was also recognised by Beacom *et al.* (1999), but was attributed to the effects of younger near-surface fluid flow associated with rifting and deposition of the overlying Stoer Group sediments.

The importance of reactivation during seismogenic slip

The Laxfordian and older structures of the Achmelvich-Clachtoll-Loch Assynt area show widespread evidence of reactivation during the ca 1.55Ga Assyntian event, with brittle deformation and frictional melting related to seismogenic slip preferentially localized along prominent pre-existing mechanical anisotropies in the basement rocks. In the case of the CSZ, the Assyntian structures are strongly localized into the region of schistose mylonites related to ductile Laxfordian deformation (Fig. 11a). The rocks here are notably finer grained and are relatively enriched in well-aligned, relatively weak and anisotropic phyllosilicate minerals such as biotite, muscovite and chlorite. Given the findings of the slip tendency analysis, which shows that the steeply dipping, ESE-WNW oriented foliation in the CSZ was favourably oriented for

slip, it is probably not surprising that the Assyntian deformation preferentially localized in this region (see also the examples discussed by Peace *et al.* 2018).

Outside of the CSZ, regionally developed features such as the Scourie dykes (Fig. 1c) are likely to represent an additional significant crustal-scale mechanical anisotropy. The observed localization of both Laxfordian and Assyntian deformation along many dyke margins - which are also in a favourable NW-SE orientation for slip – confirms that a crustal-scale anisotropy probably developed along intrusive contacts. Mantle-sourced regional dyke swarms are a common feature in basement terrains worldwide (e.g. Mackenzie dyke swarm, Canada, Hou *et al.* 2010). Given their origins as vertically oriented tensile fractures that cut much of the lithosphere, including the main load-bearing regions in the mid-crust, the localization of later regional deformation events along dyke margins is highly likely. Furthermore, many of the Scourie dyke margins were first deformed and retrogressed during Laxfordian ductile shearing, forming thin, dyke margin-parallel bands of schistose mylonite rich in weak, aligned phyllosilicates. This would likely make them even more prone to reactivation during later Assyntian strike-slip faulting.

The preferential reactivation of NW-SE dyke margins and ductile shear zone foliations is the result of strain partitioning and the development of a strong preferential alignment of slip generation surfaces and frictional melting (Fig. 11a). This highly organised configuration contrasts markedly with the patterns displayed by pseudotachylyte-bearing faults described from Lewisian rocks in the Outer Hebrides (Campbell *et al.* 2020). In the latter location, the faults show a diffuse distribution in terms of both location and orientation, a diverse range of orientations and a broad spectrum of senses of displacement including strike-slip, reverse and normal movements. This complexity may reflect a combination of superimposed deformation

events over many tens of millions of years and/or may be due the development of heterogeneous co-seismic stress field perturbations (Campbell *et al.* 2020). What is notable, however, is that widespread reactivation of pre-existing foliations by pseudotachylyte-bearing faults is not documented in the Outer Hebrides. The general absence of NW-SE steeply-dipping dyke margins and shear zone fabrics in much of the Outer Hebrides may account for the lack of Assyntian-age reactivation structures and frictional melts in this region, highlighting the integral role of pre-existing basement foliation reactivation within the Assynt Terrane and similar settings globally (e.g. Di Toro & Pennacchioni 2005).

Field observations and rock deformation experiments (e.g. see Mitchell et al. 2016) have shown that solidified friction melts can weld seismic faults making them stronger. This means that subsequent seismic ruptures may propagate along neighbouring pseudotachylyte-free slip surfaces, leading to long-term fault slip delocalization for successive ruptures. This suggestion is certainly consistent with the development of many hundreds of melt-generating slip surfaces all through the central part of the CSZ (Figs 2a, 11a) and other reactivated NW-SE shear zones in the Lewisian Gneiss Complex in mainland Scotland (e.g. see Beacom et al. 2001).

Void formation in the CSZ

The close association between slip surfaces generating friction melts (the foliation-parallel faults) and coeval dilational foliation-perpendicular faults in the CSZ requires that their development is linked to seismogenic faulting processes at > 10 km depth (Figs 11a, b). We propose that shear failure was repeatedly localized along multiple foliation planes in the favourably-oriented, highly anisotropic CSZ. It appears that simultaneous seismogenic slip and frictional melting occurred along adjacent

foliation-parallel faults, allowing long, thin (1-20 cm thick, Beacom et al. 1999, 2001) slabs of host rock to have become transiently detached from one other. We propose that these melt-lubricated slabs were simultaneously pulled apart normal to the active slip surfaces generating the foliation-perpendicular fractures, leading to instantaneous implosion of the immediate wall rocks to form localized infills of crackle to chaotic collapse-breccia (e.g. Figs 6e, f, 11bi-ii). The chaotic arrangement of the breccia clasts in many examples implies that the initial dilational cavities must have been much larger in order to allow wall rock clasts to become so misoriented and disorganized. We therefore propose that subsequent co-seismic elastic rebound led to almost instantaneous partial closure of these fault-cavities. Importantly, however, the cavities were unable to close-up completely as they were inevitably propped partially open by the infilling blocks of chaotically collapsed and misoriented wall rock (Figs 11a, b).

Developing this concept further, we speculate that the melt-lubricated blocks may have moved co-seismically at variable relative velocities as slip was accommodated along different parts of the linked array of adjacent foliation-parallel faults. This could cause the detached blocks to move apart and collide relative to one another, rapidly opening and closing the foliation-normal fracture cavities, in some cases perhaps on multiple occasions (Figs 11bi-iv). This is conceptually similar to shunting the carriages of a train, with each of the carriages represented by adjacent fault blocks, bound by the different types of fractures. Thus, if one block (carriage) was co-seismically shunted, it would move away from then adjacent block at its rear, and collide with the next adjacent block to the front, closing and opening the gaps between them (Figs 11biii. During opening, the cavity would be under a relative negative hydrostatic pressure and would draw in any available fluids, further

fragments of wall rock or frictional melt. When a cavity collapsed, larger clasts would be held in place, propping open the cavity, whilst fluids or melt would be driven out, circulating fluid (and perhaps melt) throughout the adjacent fracture network (Figs 11bii-iii). It is significant that a greater proportion of frictional melt is observed along the foliation-parallel faults in regions where there are many associated tensile fractures, compared to those areas where foliation-normal fractures are sparse. One possible reason for this is that during a seismic event, frictional melt was generated along the weak foliation-parallel faults, which lubricates multiple slip surfaces, and facilitates the block dilation and shunting process.

Comparison with other examples of pseudotachylyte-bearing faults

Pseudotachylyte occurs typically in associations of faults (or slip surfaces) and veins. The range in associations described by numerous authors (e.g. Sibson 1975; Swanson 1989; Di Toro *et al.* 2006; Nielsen *et al.* 2008; Campbell *et al.* 2020) can be usefully compared to the "block-shunting" model proposed here. The injection veins described by these authors display a wide variety of shapes and architectures, including sigmoidal and curving lenses, blebs, ladders, and networks, they are also associated with pseudotachylyte-filled breccias in seismically generated dilational jogs. These pull-apart features are in some respects similar to the foliation-normal fractures described in the present paper but exhibit two key differences. First, the dilation voids are commonly completely filled with friction melt. Second, the melt generation processes are not associated with hydrothermal mineralisation, and there is no evidence for a long-lived cavity network, such as the preservation of open vugs as seen in the present examples.

Swanson (1989) describes a process of “sidewall rip-out” development, whereby localised transient variations in frictional resistance and therefore slipping velocity along a strike-slip fault trace causes the accumulation of stresses around “statically locked” segments of a sliding fault, which if sufficient, can generate dilational tears (rip-outs) and secondary slip surfaces in the fault wall. In the examples described, the slipping surfaces generated frictional melts – which were then drawn into the rip-outs co-seismically under sub-lithostatic pressures. This has some similarity with the way in which frictional melt produced in the foliation-parallel faults at Achmelvich-Clachtoll-Loch Assynt are drawn into the abutting foliation-normal fractures as they open. Swanson (1989) further proposed that the generation of frictional melts facilitated the development of rip-outs as they lubricated the faults enabling a rapid slip-rate – this too seems generally consistent with the co-seismic block-shunting behaviour observed in the examples described here. The outcrop pattern and mechanisms described necessitate multiple fault strands to be simultaneously ruptured, with fastest displacements being able to jump across from strand to strand.

Implications for the long-term preservation of deep void networks and fluid flow

It is widely believed that substantially dilatant fracture cavities cannot exist below 1-2 km depth due to the inability of rocks to support the existence of open spaces at such high confining pressures. Our study demonstrates, however, that there is geological evidence to suggest that significant dilational cavities (cm scale) can form as co-seismic, transient features at depths >10-15 km. Furthermore, whilst they may collapse almost instantaneously, they can be preserved as partially open features due to being naturally propped open by chaotically entrained wall rock clasts. Whilst

the causative faults may become inactive, these remaining voids within linked fault arrays can then provide pipe-like pathways for the migration of fluids which likely explains their association in the Assynt terrane with at least three phases of hydrothermal mineral fills: early ubiquitous hematite, followed by quartz-epidote-prehnite and lastly calcite and zeolite). Broadly speaking this mineralization sequence is consistent with a down-temperature history of fluid flow, but this remains to be tested more rigorously. Note that only limited amounts of fault reactivation are associated with the later calcite and zeolite mineralization, suggesting a predominantly passive filling related to younger regional faulting events. This lower temperature mineralization could be related to the final stages of Assyntian activity ca 1.5 Ga (Scott 2018) or could be associated with regional faulting as recently as the Mesozoic (e.g. McCaffrey *et al.* 2020). The fact that some may still preserve open vuggy cavities suggests that a proportion of the pore spaces created in the mid-crust were never fully occluded.

More tentatively, we suggest that the proposed kinematic model in Figure 11b presents a credible mechanism for the occurrence of a 'seismogenic pumping' process at significant depths. Whilst the boundary conditions here are quite specific, it is not unreasonable to suggest that other basement terranes that see seismogenic reactivation of highly-anisotropic inherited fabrics might experience similar processes and may also see equivalent fluid or melt migration processes. For example, Holdsworth *et al.* (2019) have recently suggested that the migration of hydrothermal fluids and oil in the fractured basement reservoirs of the Rona Ridge west of Shetland was driven by a similar co-seismic pumping processes. In this sub-surface example, the authors describe naturally-propped networks of deeply-penetrating fissures within the crystalline basement of the Rona Ridge, which were buried under

a regional unconformity and charged with hydrocarbons by active rift-related seismicity (Holdsworth *et al.* 2019).

Conclusions

The development of co-seismic, fault-hosted frictional melting and transient void formation is preserved in the basement rocks of the Lewisian Complex NW Scotland and formed during Mesoproterozoic (ca 1.55 Ga) strike-slip faulting. The deformation is characterised by sinistral reactivation of pre-existing NW-SE trending Scourie dyke margins (c. 2.4Ga) and ductile shear zone fabrics (Laxfordian, ca 1.75Ga). In the CSZ, foliation-perpendicular, millimetre to decimeter-scale cavities are commonly bounded by foliation-parallel, melt-coated slip surfaces. The cavities are occupied by chaotic wall rock collapse breccias, a locally diverse range of hydrothermal minerals, and less commonly by irregular patches of injected bubbly pseudotachylyte. The development of contemporaneous foliation-parallel and -perpendicular fracture meshes appears to reflect multiscale reactivation of the steeply dipping to sub-vertical pre-existing planar fabrics and dyke contacts during strike-slip movements. Whilst frictional melts rapidly cool and weld most of the foliation-parallel slip surfaces, the chaotic fills in the linking foliation-perpendicular voids act as natural (or self-) props holding cavities open. This preserves them as sub-vertical pipe-like fluid flow conduits over long geological time periods, as illustrated by the widespread development of broadly down-temperature hydrothermal mineralization in these brecciated cavities. The examples illustrate that mid-crustal void formation may initiate potentially very long-lived percolation pathways that are able to host later episodes of hydrothermal fluid flow and mineralization even if the hosting faults are not significantly reactivated.

Acknowledgements:

Thanks go to the Geological Society of London for their generous support of the research through the Annie Greenly Grant, and for publishing the field diary for this research in the *Geoscientist* magazine. We are grateful to the Tectonic Studies Group (TSG) for their travel bursary allowing the first author to present their work and gain valuable feedback from peers. The publishing of this work is funded by the Journal of the Geological Society ECR open-access prize. Thanks also go to all field assistants and helpers, and the authors ever-patient partners.

REFERENCES CITED

Allmendinger, R.W., Cardozo, N. & Fisher, D.M. 2011. *Structural Geology Algorithms: Vectors and Tensors*. Cambridge University Press, https://doi.org/10.1017/CBO9780511920202.

Angelier, J. & Mechler, P. 1977. Sur une methode graphique de recherche des contraintes principales egalement utilisables en tectonique et en seismologie : la methode des diedres droits. *Bulletin de la Societe Geologique de France*, **S7-XIX**, 1309–1318, https://doi.org/10.2113/gssgfbull.S7-XIX.6.1309.

Attfield, P. 1987. The structural history of the Canisp Shear Zone. *Geological Society, London, Special Publications*, **27**, 165–173, https://doi.org/10.1144/GSL.SP.1987.027.01.14.

Beacom, L.E., Anderson, T.B. & Holdsworth, R.E. 1999. Using basement-hosted clastic dykes as syn-rifting palaeostress indicators: an example from the basal Stoer Group, northwest Scotland. *Geol. Mag*, **136**, 301–310.

Beacom, L.E., Holdsworth, R.E., McCaffrey, K.J.W. & Anderson, T.B. 2001. A quantitative study of the influence of pre-existing compositional and fabric heterogeneities upon fracture-zone development during basement reactivation. *Geological Society Special Publication*, **186**, 195–211, https://doi.org/10.1144/GSL.SP.2001.186.01.12.

Bott, M.H.P. 1959. The Mechanics of Oblique Slip Faulting. *Geological Magazine*, **XCVI**, 109–117, https://doi.org/10.1017/S0016756800059987.

Campbell, L.R., Lloyd, G.E., Phillips, R.J., Walcott, R.C. & Holdsworth, R.E. 2020. Stress fields of ancient seismicity recorded in the dynamic geometry of pseudotachylyte in the Outer Hebrides Fault Zone, UK. *Journal of the Geological Society*, jgs2020-101, https://doi.org/10.1144/jgs2020-101.

Chapman, H.J. 1979. 2,390 Myr Rb-Sr whole-rock for the Scourie dykes of north-west Scotland [6]. *Nature*, **277**, 642–643, https://doi.org/10.1038/277642a0.

Chattopadhyay, A., Holdsworth, R.E., McCaffrey, K.J.W. & Wilson, R.W. 2010. Recording and analyzing geospatially accurate structural data through 'digital mapping' technique: A case study from the Canisp Shear Zone, NW Scotland. *Journal of the Geological Society of India*, **75**, 43–59, https://doi.org/10.1007/s12594-010-0023-y.

Cheng, C., Milsch, H. 2021. Hydromechanical Investigations on the Self-propping Potential of Fractures in Tight Sandstones. *Rock Mechanics and Rock Engineering*, **54,** 5407–5432. https://doi.org/10.1007/s00603-021-02500-4

Chernov, A.A., Kedrinsky, V.K. & Pil'nik, A.A. 2014. Kinetics of Phase Change. II Transformation-Time Relations for Random Distribution of. *Physics of Fluids*,

26, https://doi.org/10.1063/1.4900846.
Corfu, F., Heaman, L.M. & Rogers, G. 1994. Polymetamorphic evolution of the Lewisian complex, NW Scotland, as recorded by U-Pb isotopic compositions of zircon, titanite and rutile. *Contributions to Mineralogy and Petrology*, **117**, 215–228, https://doi.org/10.1007/BF00310864.
Davies, J.H.F.L. & Heaman, L.M. 2014. New U-Pb baddeleyite and zircon ages for the Scourie dyke swarm: A long-lived large igneous province with implications for the Paleoproterozoic evolution of NW Scotland. *Precambrian Research*, **249**, 180–198, https://doi.org/10.1016/j.precamres.2014.05.007
Davis, T., Healy, D., Bubeck, A. and Walker, R. 2017. Stress concentrations around voids in three dimensions: The roots of failure. *Journal of Structural Geology*, **102,** 193–207, https://doi.org/10.1016/j.jsg.2017.07.013
Delvaux, D. & Sperner, B. 2003. New aspects of tectonic stress inversion with reference to the TENSOR program. *Geological Society Special Publication*, **212**, 75–100, https://doi.org/10.1144/GSL.SP.2003.212.01.06.
Dempsey, E.D., Holdsworth, R.E., Imber, J., Bistacchi, A. & Di Toro, G. 2014. A geological explanation for intraplate earthquake clustering complexity: The zeolite-bearing fault/fracture networks in the Adamello Massif (Southern Italian Alps). *Journal of Structural Geology*, **66**, 58–74, https://doi.org/10.1016/j.jsg.2014.04.009.
Di Toro, G. & Pennacchioni, G. 2005. Fault plane processes and mesoscopic structure of a strong-type seismogenic fault in tonalites (Adamello batholith, Southern Alps). *Tectonophysics*, **402**, 55–80, https://doi.org/10.1016/j.tecto.2004.12.036.
Di Toro, G., Hirose, T., Nielsen, S., Pennacchioni, G. & Shimamoto, T. 2006. Natural and experimental evidence of melt lubrication of faults during earthquakes. *Science*, **311**, 647–649, https://doi.org/10.1126/science.1121012.
Evans, C.R. & Lambert, R. St J. 1974. The Lewisian of Lochinver, Sutherland; the type area for the Inverian metamorphism. Journal of the Geological Society,130(2):125. http://dx.doi.org/10.1144/gsjgs.130.2.0125
Fagereng, Å. & Toy, V.G. 2011. Geology of the earthquake source: An introduction. *Geological Society Special Publication*, **359**, 1–16, https://doi.org/10.1144/SP359.1.
Friend, C.R.L. & Kinny, P.D. 1995. New evidence for protolith ages of Lewisian granulites, northwest Scotland. *Geology*, **23**, 1027–1030, https://doi.org/10.1130/0091-7613(1995)023<1027:nefpao>2.3.co;2.
Goodenough, K.M., Crowley, Q.G., Krabbendam, M. & Parry, S.F. 2013. New U-Pb age constraints for the Laxford Shear Zone, NW Scotland: Evidence for tectono-magmatic processes associated with the formation of a Paleoproterozoic supercontinent. *Precambrian Research*, **233**, 1–19, https://doi.org/10.1016/j.precamres.2013.04.010.
Guice, G.L., McDonald, I., Hughes, H.S.R., MacDonald, J.M. & Faithfull, J.W. 2020. Origin(s) and geodynamic significance of Archean ultramafic–mafic bodies in the mainland Lewisian Gneiss Complex, North Atlantic Craton. *Journal of the Geological Society*, jgs2020-013, https://doi.org/10.1144/jgs2020-013.
Hardman, K., Holdsworth, R.E., Dempsey, E. & Mccaffrey, K. 2020. Nature and significance of rift-related, near-surface fissure-fill networks in fractured carbonates below regional unconformities, https://doi.org/10.6084/m9.figshare.c.5023103.
Heaman, L.M. & Tarney, J. 1989. U-Pb baddeleyite ages for the Scourie dyke

swarm, Scotland: Evidence for two distinct intrusion events. *Nature*, **340**, 705–708, https://doi.org/10.1038/340705a0.

Holdsworth, R.E., McCaffrey, K.J.W., et al. 2019. Natural fracture propping and earthquake-induced oil migration in fractured basement reservoirs. *Geology*, **47**, 700–704, https://doi.org/10.1130/G46280.1.

Holdsworth, R.E., Trice, R., et al. 2020a. The nature and age of basement host rocks and fissure fills in the Lancaster field fractured reservoir, West of Shetland. *Journal of the Geological Society*, https://doi.org/10.6084/m9.

Holdsworth, R.E., Selby, D., Dempsey, E., Scott, L., Hardman, K., Fallick, A.E. & Bullock, R. 2020b. The nature and age of Mesoproterozoic strike-slip faulting base on Re-Os geochronology of syntectonic copper mineralisation, Assynt Terrane, NW Scotland. *Journal of the Geological Society of London*.

Holland, M., Urai, J.L. & Martel, S. 2006. The internal structure of fault zones in basaltic sequences. *Earth and Planetary Science Letters*, **248**, 286–300, https://doi.org/10.1016/j.epsl.2006.05.035.

Holland, M., van Gent, H., Bazalgette, L., Yassir, N., Hoogerduijn Strating, E.H. & Urai, J.L. 2011. Evolution of dilatant fracture networks in a normal fault - Evidence from 4D model experiments. *Earth and Planetary Science Letters*, **304**, 399–406, https://doi.org/10.1016/j.epsl.2011.02.017.

Hou, G., Kusky, T.M., Wang, C. & Wang, Y. 2010. Mechanics of the giant radiating Mackenzie dyke swarm: A paleostress field modeling. *Journal of Geophysical Research*, **115**, B02402, https://doi.org/10.1029/2007JB005475.

Jensen, L.N. 1984. Quartz microfabric of the Laxfordian Canisp Shear Zone, NW Scotland. *Journal of Structural Geology*, https://doi.org/10.1016/0191-8141(84)90053-1.

Kinny, P.D., Friend, C.R.L., Strachan, R.A., Watt, G.R. & Burns, I.M. 1999. U-Pb geochronology of regional migmatites in East Sutherland, Scotland: Evidence for crustal melting during the Caledonian orogeny. *In*: *Journal of the Geological Society*. Geological Society of London, 1143–1152., https://doi.org/10.1144/gsjgs.156.6.1143.

Kirkpatrick, J.D. & Rowe, C.D. 2013. Disappearing ink: How pseudotachylytes are lost from the rock record. *Journal of Structural Geology*, **52**, 183–198, https://doi.org/10.1016/j.jsg.2013.03.003.

Lisle, R.J. & Srivastava, D.C. 2004. Test of the frictional reactivation theory for faults and validity of fault-slip analysis. *Geology*, **32**, 569–572, https://doi.org/10.1130/G20408.1.

Love, G.J., Kinny P. D. & Friend, C.R.L. 2004. Timing of magmatism and metamorphism in the Gruinard Bay area of the Lewisian Gneiss Complex: comparisons with the Assynt Terrane and implications for terrane accretion. *Contrib. Mineral Petrol*, **146**, 620–636, https://doi.org/10.1007/s00410-003-0519-1.

MacDonald, J.M., Goodenough, K.M., Wheeler, J., Crowley, Q., Harley, S.L., Mariani, E. & Tatham, D. 2015. Temperature-time evolution of the Assynt Terrane of the Lewisian Gneiss Complex of Northwest Scotland from zircon U-Pb dating and Ti thermometry. *Precambrian Research*, **260**, 55–75, https://doi.org/10.1016/j.precamres.2015.01.009.

McCaffrey, K.J.W**.** Holdsworth, R.E. Pless, J. Franklin, B.S.G. & Hardman, K 2020. Basement reservoir plumbing: Fracture aperture, length and topology analysis of the Lewisian Complex, NW Scotland. Journal of the Geological Society **177**, 1281-1293.

Morris, A., Ferrill, D.A. & Henderson, D.B. 1996. Slip-tendency analysis and fault reactivation. *Geology*, **24**, 275–278, https://doi.org/10.1130/0091-7613(1996)024<0275:STAAFR>2.3.CO;2.

Nielsen, S., Di Toro, G., Hirose, T. & Shimamoto, T. 2008. Frictional melt and seismic slip. *Journal of Geophysical Research*, **113**, B01308, https://doi.org/10.1029/2007JB005122.

Park, R.G. 1970. Observations on Lewisian Chronology.

Park, R.G. 2005. The Lewisian terrane model: a review. *Scottish Journal of Geology*, **41**, 105–118.

Park, R.G. & Tarney, J. 1987. The Lewisian complex: a typical Precambrian high-grade terrain? *Geological Society, London, Special Publications*, **27**, 13–25, https://doi.org/10.1144/gsl.sp.1987.027.01.03.

Park, R.G., Cliff, R.A., Fettes, D.J. & Stewart, A.D. 1994. Precambrian rocks in northwest Scotland west of the Moine Thrust. *In*: *A Revised Correlation of Pre-Cambrian Rocks in the British Isles*. Geological Society of London, 6–22., https://doi.org/10.1144/sr22.2.

Passchier, C.W. & Trouw, R.A.J. 2005. *Microtectonics*, 2nd ed. Berlin, Springer-Verlag Berlin Heidelberg.

Peace, A., McCaffrey, K., Imber, J., van Hunen, J., Hobbs, R. & Wilson, R. 2018. The role of pre-existing structures during rifting, continental breakup and transform system development, offshore West Greenland. *Basin Research*, **30**, 373–394, https://doi.org/10.1111/bre.12257.

Petit, J.P. 1987. Criteria for the sense of movement on fault surfaces in brittle rocks. *Journal of Structural Geology*, **9**, 597–608, https://doi.org/10.1016/0191-8141(87)90145-3.

Rowe, C.D., Ross, C., et al. 2018. Geometric Complexity of Earthquake Rupture Surfaces Preserved in Pseudotachylyte Networks. *Journal of Geophysical Research: Solid Earth*, **123**, 7998–8015, https://doi.org/10.1029/2018JB016192.

Sanderson, D.J. & Nixon, C.W. 2015. The use of topology in fracture network characterization. *Journal of Structural Geology*, **72**, 55–66, https://doi.org/10.1016/j.jsg.2015.01.005.

Scott, L.J. 2018. *Dyke Reactivation across the Frictional-Viscous Transition: Precambrian Deformation of Scourie Dyke Margins in NW Scotland*. Durham University.

Sheraton, J., Skinner, A. & Tarney, J. 1973. The Geochemistry of the Scourian gneisses of the Assynt district. *In*: Park, R. & Tarner, J. (eds) *The Early Precambrian of Scotland and Related Rocks of Greenland*. Keele, University of Keele, 13–30., https://doi.org/10.1007/BF00373779.RIS.

Sibson, R.H. 1975. Generation of Pseudotachylyte by Ancient Seismic Faulting. *Geophysical Journal of the Royal Astronomical Society*, **43**, 775–794, https://doi.org/10.1111/j.1365-246X.1975.tb06195.x.

Sibson, R.H. 1993. Load-strengthening versus load-weakening faulting. *Journal of Structural Geology*, **15**, 123–128, https://doi.org/10.1016/0191-8141(93)90090-W.

Sibson, R.H. & Toy, V.G. 2006. The habitat of fault-generated pseudotachylyte: Presence vs. absence of friction-melt. *In*: *Geophysical Monograph Series*. Blackwell Publishing Ltd, 153–166., https://doi.org/10.1029/170GM16.

Stewart, A.D. 1993. Late Proterozoic and Late Palaeozoic movement on the Coigach fault in N W Scotland. *Scottish Journal of Geology*, **29**, 21–28.

Sutton, J. & Watson, J. 1951. The pre-Torridonian metamorphic history of the Loch

Torridon and Scourie areas in the North-West Highlands, and its bearing on the chronological classification of the Lewisian. *Quarterly Journal of the Geological Society of London*, **106**, 241–307, https://doi.org/10.1144/GSL.JGS.1950.106.01-04.16.

Swanson, M.T. 1989. Sidewall ripouts in strike-slip faults. *Journal of Structural Geology*, **11**, 933–948, https://doi.org/10.1016/0191-8141(89)90045-X.

Tarney, J. 1963. Assynt dykes and their metamorphism. *Nature*, **199**, 672–674.

Tavani, S., Granado, P., et al. 2014. Building a virtual outcrop, extracting geological information from it, and sharing the results in Google Earth via OpenPlot and Photoscan: An example from the Khaviz Anticline (Iran). *Computers and Geosciences*, **63**, 44–53, https://doi.org/10.1016/j.cageo.2013.10.013.

Ukar, E., Baqués, V., Laubach, S. E., and Marrett, R. 2020. The nature and origins of decameter-scale porosity in Ordovician carbonate rocks, Halahatang oilfield, Tarim Basin, China, *Journal of the Geological Society, London*, **177**, 1074–1091, https://doi.org/10.1144/jgs2019-156

van Gent, H.W., Holland, M., Urai, J.L. & Loosveld, R. 2010. Evolution of fault zones in carbonates with mechanical stratigraphy - Insights from scale models using layered cohesive powder. *Journal of Structural Geology*, **32**, 1375–1391, https://doi.org/10.1016/j.jsg.2009.05.006.

Vernon, R., Holdsworth, R.E., Selby, Dempsey, D., Finlay, E. & Fallick, A.J. 2014. Structural characteristics and Re–Os dating of quartz-pyrite veins in the Lewisian Gneiss Complex, NW Scotland: Evidence of an Early Paleoproterozoic hydrothermal regime during terrane amalgamation. *Precambrian Research*, **246**, 256–267, https://doi.org/10.1016/j.precamres.2014.03.007.

Wallace, R.E. 1951. Geometry of Shearing Stress and Relation to Faulting. *The Journal of Geology*, **59**, 118–130, https://doi.org/10.1086/625831.

Weismüller, C., Urai, J.L., Kettermann, M., von Hagke, C. & Reicherter, K. 2019. Structure of massively dilatant faults in Iceland: lessons learned from high-resolution unmanned aerial vehicle data. *Solid Earth*, **10**, 1757–1784, https://doi.org/10.5194/se-10-1757-2019.

Wheeler, J., Park, R.G., Rollinson, H.R. & Beach, A. 2010. The Lewisian Complex: Insights into deep crustal evolution. *Geological Society Special Publication*, **335**, 51–79, https://doi.org/10.1144/SP335.4.

Whitehouse, M.J. 1989. Sm-Nd evidence for diachronous crustal accretion in the Lewisian Complex of Northwest Scotland. In: L.D. Ashwal (editor), Growth of the Continental Crust, *Tectonophysics* **161**, 245-56.

Whitehouse, M.J. & Kemp, A.I.S. 2010. On the difficulty of assigning crustal residence, magmatic protolith and metamorphic and ages to Lewisian granulites – constraints from combined in situ U-Pb and Lu-Hf. *In:* Law, R.D., Butler, R.W.H., Holdsworth, R., Krabbendam, M. and Strachan R. (editors). *Continental Tectonics and Mountain Building: The Legacy of Peach and Horne.* Geological Society of London Special Publications **335,** 81-101

Whitehouse, M.J., Kemp, A.I.S. & Petersson, A. 2022. Persistent mildly supra-chondritic initial Hf in the Lewisian Complex, NW Scotland: implications for Neoarchean crust-mantle differentiation *Chemical Geology* 606, 121001.

Wilson, R., Holdsworth, R.E. & Wightmand, R. 2011. Transect through the Canisp Shear Zone, Achmelvich, North-west Highlands - an excursion. Excursion 2. *In*: Goodenough, K. M. & Krabbendam, M. (eds) *A Geological Excursion Guide to the North-West Highlands of Scotland.* . Edinborogh, Edinborugh Geological Society, 53–61.

Woodcock, N.H. & Mort, K. 2008. Classification of fault breccias and related fault rocks. *Geological Magazine*, **145**, 435–440, https://doi.org/10.1017/S0016756808004883.
Xu, W., Feng, G., Meng, L., Zhang, A., Ampuero, J.P., Bürgmann, R. & Fang, L. 2018. Transpressional Rupture Cascade of the 2016 Mw 7.8 Kaikoura Earthquake, New Zealand. *Journal of Geophysical Research: Solid Earth*, **123**, 2396–2409, https://doi.org/10.1002/2017JB015168.
Zhu, X.K., O'Nions, R.K., Belshaw, N.S. & Gibb, A.J. 1997. Lewisian crustal history from in situ SIMS mineral chronometry and related metamorphic textures. *Chemical Geology*, **136**, 205–218, https://doi.org/10.1016/S0009-2541(96)00143-X.

FIGURE

a) Simplified terrane map of the Lewisian complex W of the Moine Thrust. b) Map showing local extent of the Scourie dyke swarm, adapted from Holdsworth *et al.* (2020b) c) Geological map of the Assyntian Terrane with hill shaded topography showing the Stoer and Canisp shear zones, and major faults. Location maps, digital data provided with permission by EDINA Digimap (OS Terrain 5 [ASC & SHAPE geospatial data] scale 1:10000, tiles NB92, NB91, NC01-03, NC11-13, NC21-23, NC31-33, updated April 2021, Ordnance Survey (GB), and DiGMapGB-50 [SHAPE geospatial data], scale 1:250000, tiles NB92, NB91, NC01-03, NC11-13, NC21-23, NC31-33, updated April 2021, BGS, using EDINA Geology Digimap Service, https://digimap.edina.ac.uk).

Figure 2) Summary of pre-Assyntian ductile fabrics including representative field-photographs, structural orientations, and location map. a) Location map showing the zonation of the Canisp Shear Zone at Achmelvich Bay and location of key Scourie dykes and structural data sources. b) Above: Field photograph of Badcallian foliation and schlieren textures around a mafic enclave (highlighted in white; NC 0563 2500). Below: Lower hemisphere stereographic projection of Badcallian planar fabrics and

lineation data, collected from outside the Canisp Shear Zone. c) Above: Field photograph of Inverian foliation and folding (highlighted in white; NC 0575 2553). Below: Lower hemisphere stereographic projection of Inverian planar fabrics and lineation data, collected from the outer parts of the Canisp Shear Zone. d) Above: Field photograph of Laxfordian foliation (highlighted in white; NC 0572 2554). Lower hemisphere stereographic projection of Laxfordian planar fabrics and lineation data, collected from reactivated dyke contacts and central part of the Canisp Shear Zone.

Figure 3) Summary of dyke margin reactivation during the Laxfordian event. a) Hill shaded topographic and satellite map of Achmelvich beach showing the present-day locations of two prominent Scourie dykes (purple) and surrounding structures. Data used with permission by EDINA Digimap (Aerial digimap, 25cm resolution, 2018). Grid squares = $100m^2$. b) Field photograph of gneiss xenolith within the northernmost dyke in map 3a. Gneissic foliation highlighted in white, and margins in yellow (NC 0565 2507. c) Field photograph of a ductile dextral sheared dyke margin from S side of Achmelvich beach, highlighting the development of cm-wide schistose shear fabrics (white dotted line) close to the pre-existing igneous contact (yellow dotted line; NC 0546 2490) d) Field photograph of ductile dextrally sheared dyke margin, highlighting the development of asymmetrical schistose fabrics (white dotted line) either side of the pre-existing igneous contact (yellow dotted line; NC 0570 2512) e) Field photograph of asymmetric shear fabrics wrapping a pre-existing ultra-mafic pod (NC0473 2659). f) Thin section photomicrograph under plain polarized light (PPL) of dextral S-C' (yellow and green) banding fabrics within the dyke-margin biotite muscovite schists.

Figure 4) Field photographs and maps summarising the dyke margin and shear zone reactivation structures of the Assynt Terrane. a) Location map showing the detailed zonation within the Canisp Shear Zone and locations of field photographs. For key see Fig. 2a. b) Plan view field photographs of foliation-parallel sinistral faults with breccia & haematite staining in schistose Laxfordian mylonites (NC 0572 2554) c) Field photograph of Inverian foliation and tight isoclinal folding (white) cut by foliation-parallel Assyntian faulting (yellow) associated with frictional melts – pseudotachylyte (PT; NC 0416 2655). d) Field photograph of dyke margin Laxfordian ultramylonites in plan view overprinted by sinistral shear associated with epidote mineralization, Loch Assynt shore (NC 2104 2519). e) Field photograph from the same location as (d) showing detailed view of reactivated dyke margin contact highlighting sheared nature of epidote mineralization. f) Thin section scan view and interpretation of dyke margin fabric taken at the Loch Assynt shoreline (after Holdsworth *et al*. 2020b). Section shows Assyntian ultramylonitic fabric with sinistral minor folds (blue), S-C fabrics, and asymmetrically wrapped porphyroclasts, overprinted by sinistral cataclasites (brown), pseudotachylytes (PT), brittle faulting (red), and development of quartz-epidote mineralized slickenlines and attritional breccias (green). This tracks the development of dyke margin fabric across the frictional-viscous transition during the Assyntian. g) Field photograph of slickenlines indicating sinistral shear sense on a NW-SE trending foliation parallel fault surface (NC 0575 2554). h) Plan view field photograph of steeply plunging sinistral brittle-ductile folding associated with foliation-parallel detachments (yellow) with hematite staining in schistose Laxfordian mylonite. Trace of folded foliation shown in white (NC 0572 2554).

Figure 5) Field photographs of sediment-filled faults and fractures. a) Field photograph showing the sediment-filled fracture array highlighted in yellow (NC 0409 2659. b) Field photograph of sediment-filled fracture from the south side of Achmelvich Bay (NC 0534 2495).

Figure 6) Field photographs and orientation data from Alltan Na Bradhan and Cathair Dhubh outcrops, showing Assyntian fault architectures. Zones of foliation-perpendicular fractures are outlined in yellow, foliation planes and parallel shear faults are outlined in white. a) Lower hemisphere stereographic projection of Assyntian fault planes. Data are divided into faults showing dextral (blue) and sinistral (red) offsets and are contoured independently and to the same scale. Poles to fault planes shown as circles with mean planes plotted and fault slip vectors as diamonds. Large black dot is the intersection lineation between sinistral and dextral mean fault planes. The mean Laxfordian foliation plane (from Fig. 2d) is also shown in black for reference. Kinematic data from these faults are shown in Fig. 9. b) Oblique field photograph of foliation-perpendicular 'ladder' fracture zone with pervasive haematite staining, multiple fractures and crackle breccias (NC 0483 2620) c) Oblique aerial image taken using a drone of the Port Alltan na Bradhan outcrop showing the large length, high intensity, and minimal damage zone of the foliation-parallel Assyntian fractures (NC 0483 2620). d) Cross section view in field photograph of foliation-parallel fault, featuring single discrete slip surface and minor damage zone on one fault wall (NC 0575 2553). e) Plan view field photograph showing breccia-filled foliation perpendicular fracture filled with chaotically rotated clasts and intra-clast void spaces (NC 0573 2554). f) Field photograph in plan view of dilatant breccia-filled fracture, note the foliation-parallel opening vector orientation

(NC 0573 2554). g) Cut sample showing chaotic, clast-supported nature of breccias, strong haematite staining and patches of injected pseudotachylyte.

Figure 7) Field photographs and photomicrographs of pseudotachylyte-bearing structures. a) Plan view of composite pseudotachylyte injection vein and breccia showing numerous “wing cracks” consistent with sinistral shear (NC 0415 2657). b) Thin section photomicrograph in plane polarized light of devitrified pseudotachylyte showing dendritic-spherulitic silica microcrystallites set in an amorphous melt. c) Cross section view of large wing crack / injection vein of pseudotachylyte (outlined in red) emanating from a foliation-parallel fault (highlighted in white) (NC 0483 26200). d) Section view of pseudotachylyte in sub-vertical fault plane showing flow textures wrapping around fault plane asperities (NC 0575 2553). e) Thin section photomicrograph in plane polarized light of flow structures within colour-baanded composite pseudotachylyte. f) Thin section photomicrograph in plane polarized light of ‘wing crack’ injection into crystalline gneissic wall rock. g) Close up field photograph showing breccia with clasts of wall rock and early pseudotachylyte set in a matrix of younger pseudotachylyte melt (NC 0420 2657). h) Thin section photomicrograph in plane polarized light of vesicles and amygdales in pseudotachylyte.

Figure 8) Field photographs and thin sections of breccia fills. a) Field photograph of breccia filled foliation-perpendicular fracture (yellow) showing large cavities between clasts, abutting against foliation parallel faults (white) (NC 0483 2620). b) Field photograph of foliation-perpendicular fault filled with angular clasts of wall rock set in an epidote cemented matrix (NC 0482 2621). c) Thin section photomicrograph in

cross polars showing void spaces and syntaxial mineral growths of cementing prehnite. d) Thin section photomicrograph in plane polarized light of fault breccia showing haematite rims and cements around wall rock clasts. e) Thin section photomicrograph in plane polarized light of epidote-rich breccia-cataclasite between gneissic wall rock. f) Field photograph of plan view of filled fault cavity showing multiple successive infills as distinguished by different clast types and mineral cements; earlier hematite cemented units are cut by later epidote cemented fault rocks (NC 0482 2621). g) Field photograph of foliation-parallel fault with preserved slickenlines showing epidote and hematite mineralized surfaces (NC 0482 2621).

Figure 9) Summary of inverted palaeostress axis orientations from slickenline data. In all cases, the data have been back-rotated to remove the regional tilt displayed by the immediately overlying Stoer Group (see Holdsworth et al 2020b). Note that the sub-vertical orientation of sigma 2 is consistent with the proposed strike-slip regime. a) Lower hemisphere stereographic projection of right dihedron palaeostress inversion results from all Assyntian outcrops. b) Lower hemisphere stereographic projection showing the results of right dihedron palaeostress inversion from the Cathair Dhubh outcrop. c) Stereographic projection showing results of normalised slip tendency analysis showing critically stressed E-W structures. d) Lower hemisphere stereographic projection of contoured poles to observed tensile fault planes. e) Schematic plan-view illustration showing the orientations of Assyntian faults and fractures in relation to Riedel secondary shear classifications – R, R', Y, T.

Figure 10) Summary of fault topology from virtual outcrop models, after Sanderson and Nixon (2015). a) Sample windows and topology superimposed onto a

planimetrically correct orthorectified outcrop model of Alltan Na Bradhan. Right, topological results plotted onto a ternary diagram (Sanderson & Nixon 2015) b) Sample windows and topology superimposed onto a planimetrically correct orthorectified outcrop model of Cathair Dhubh. c) Summary of node and branch classifications from outcrops shown. d) Maximum magnification of model in (b) showing the resolution of the model and extreme density of fractures present including uninterpreted fractures below viewing resolution during interpretation.

Figure 11) a) Summary 'static' 3D model of Assyntian reactivation structures (faults, fractures, fault rocks, mineralization) seen in the centre of the Canisp Shear Zone and the general relationship to sinistral shearing and the causative stresses (illustrated using sigma 1 and 3 for reference). b)i-iv) Dynamic illustrative plan-view illustrations of sequential development and interactions of Assyntian structures showing the proposed block-shunting processes and relationships to frictional melting and fluid flow. Note that the sequences may repeat and not always in the same order as indicated by the black arrows connecting boxes. See text for further details.

Figure 1

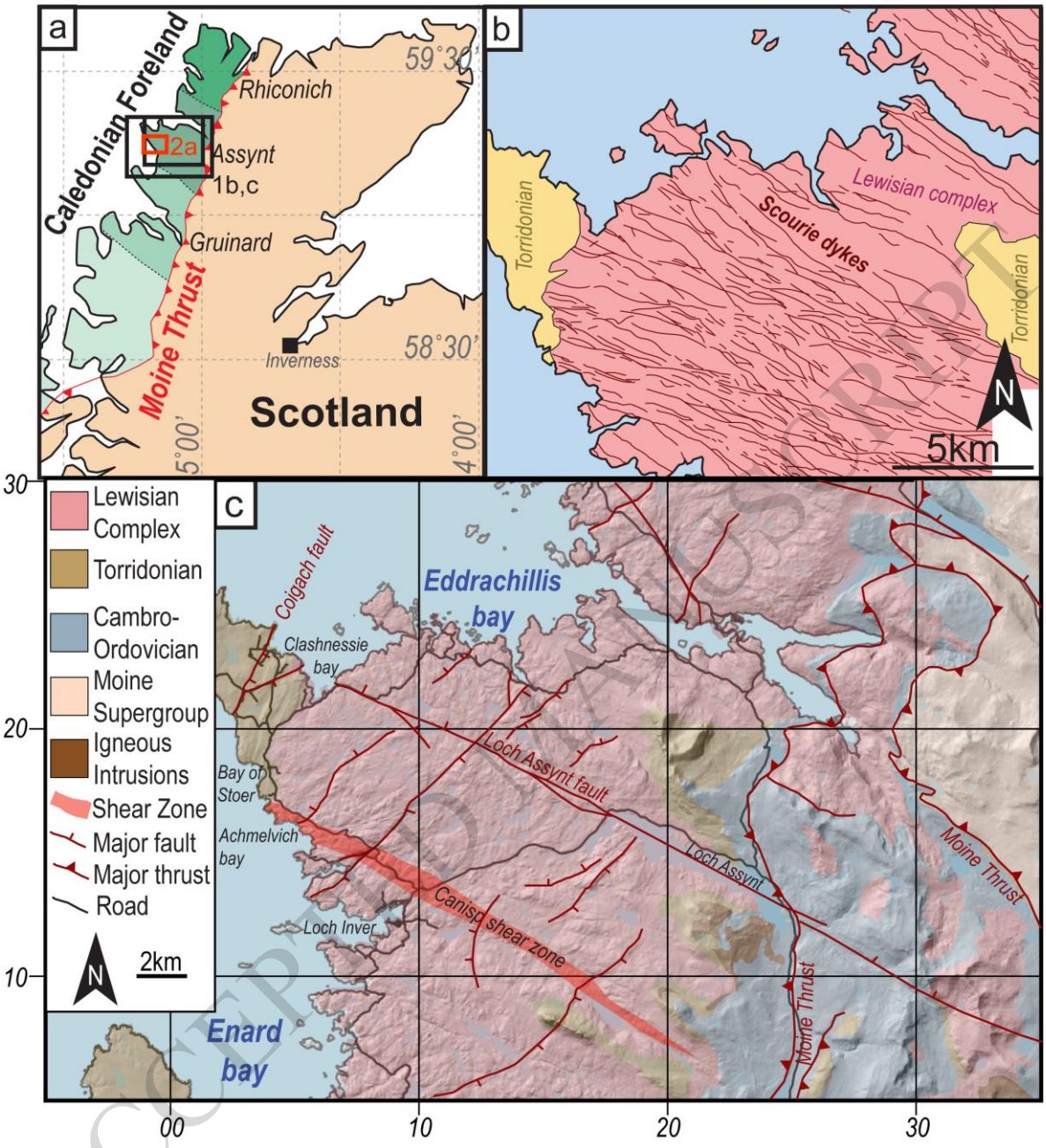

Figure 2

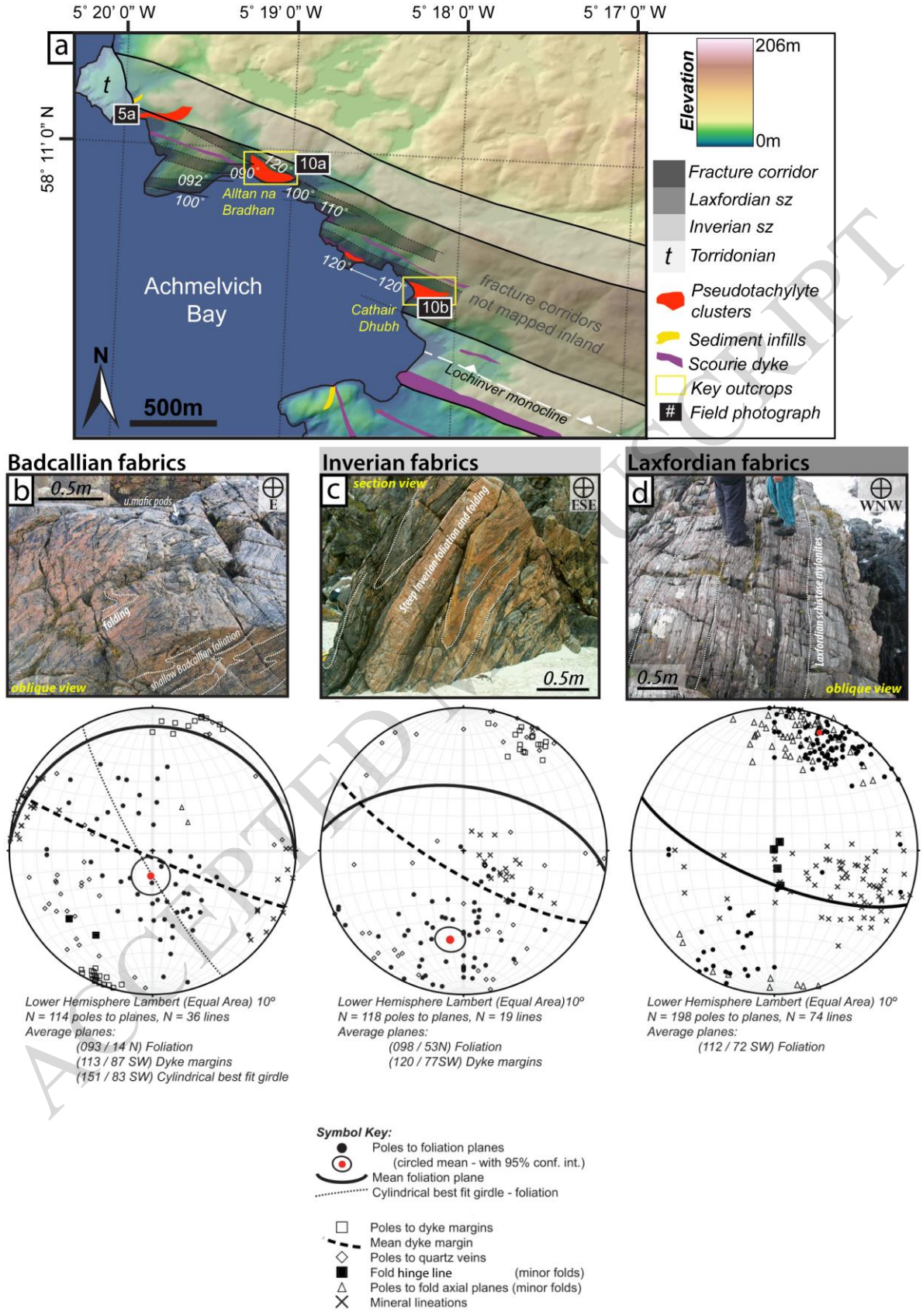

Lower Hemisphere Lambert (Equal Area) 10°
N = 114 poles to planes, N = 36 lines
Average planes:
(093 / 14 N) Foliation
(113 / 87 SW) Dyke margins
(151 / 83 SW) Cylindrical best fit girdle

Lower Hemisphere Lambert (Equal Area)10°
N = 118 poles to planes, N = 19 lines
Average planes:
(098 / 53N) Foliation
(120 / 77SW) Dyke margins

Lower Hemisphere Lambert (Equal Area) 10°
N = 198 poles to planes, N = 74 lines
Average planes:
(112 / 72 SW) Foliation

Figure 3

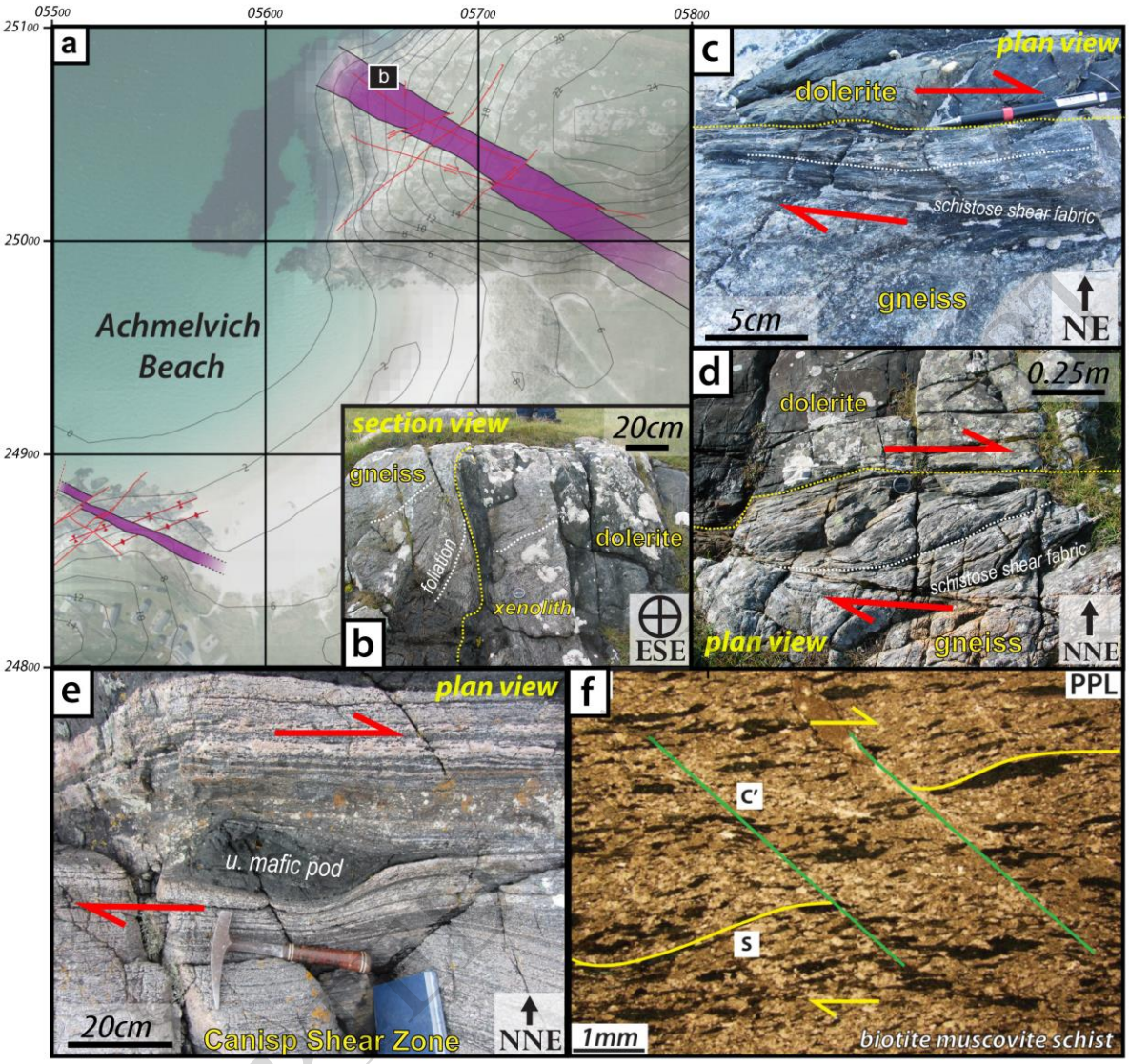

Figure 4

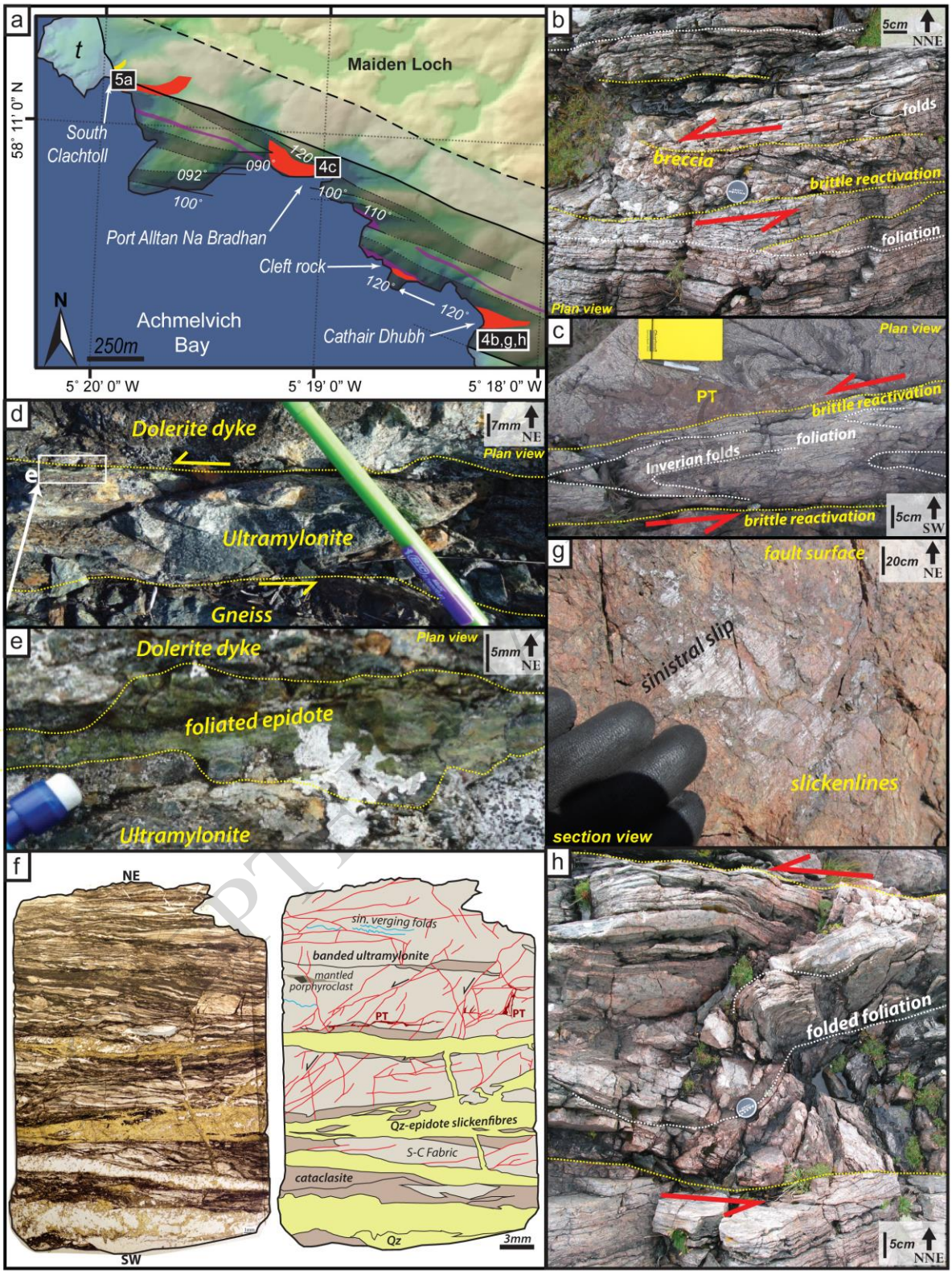

Figure 5

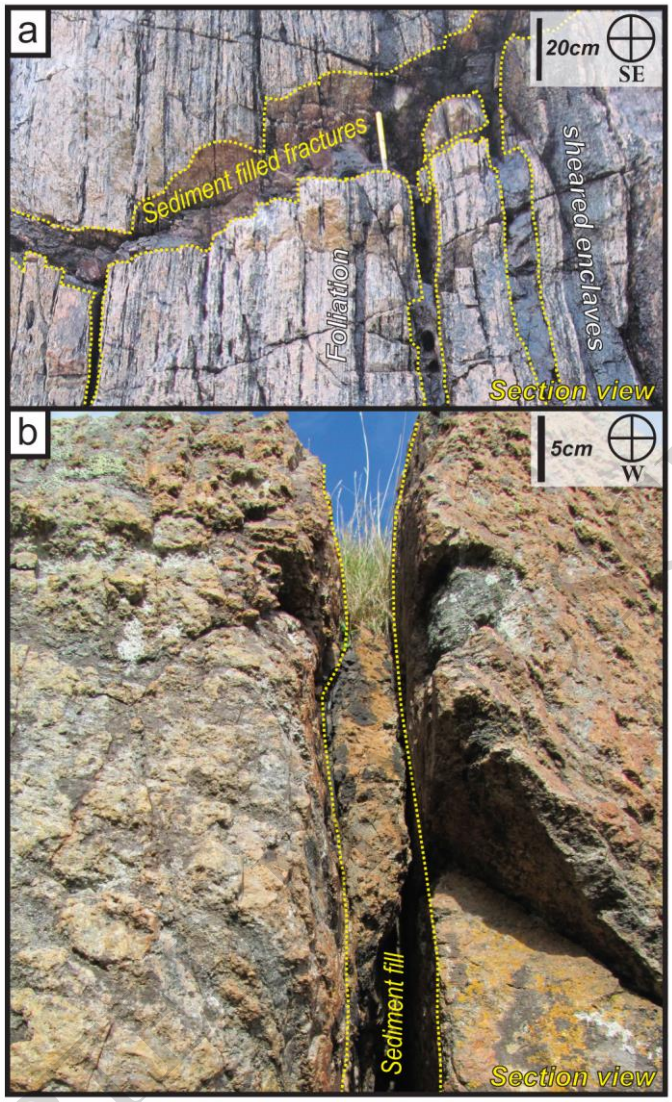

Figure 6

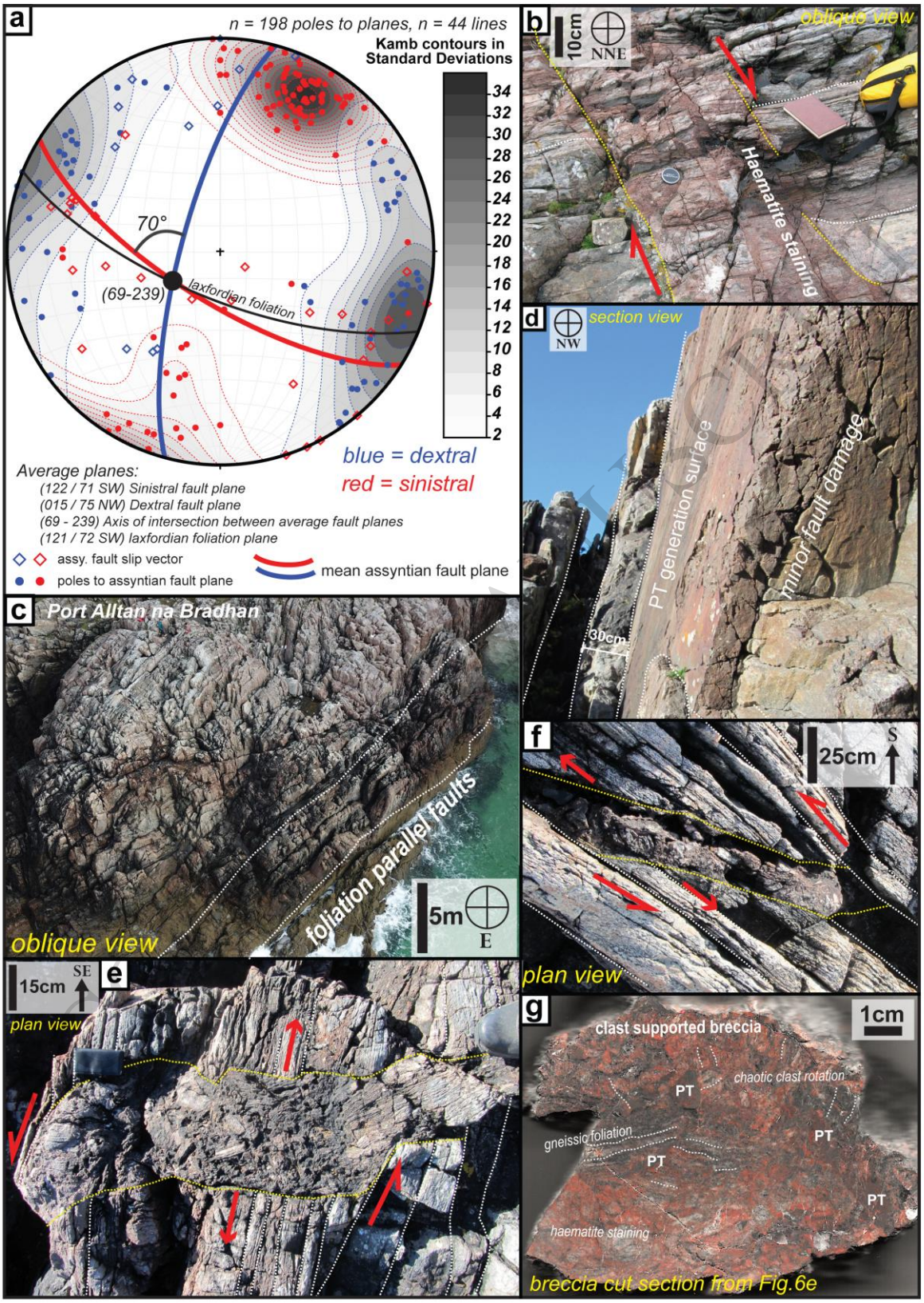

Figure 7

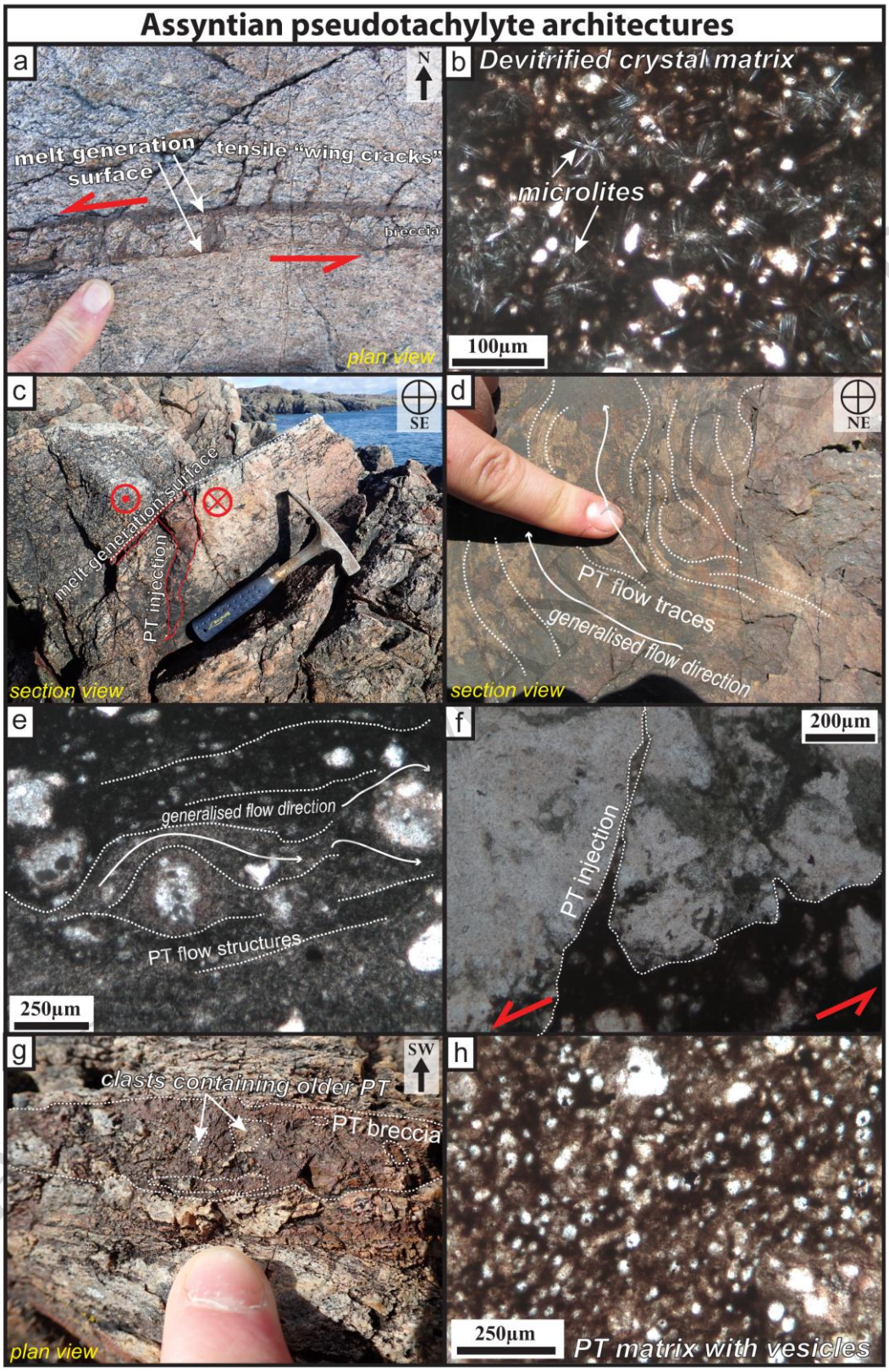

Figure 8

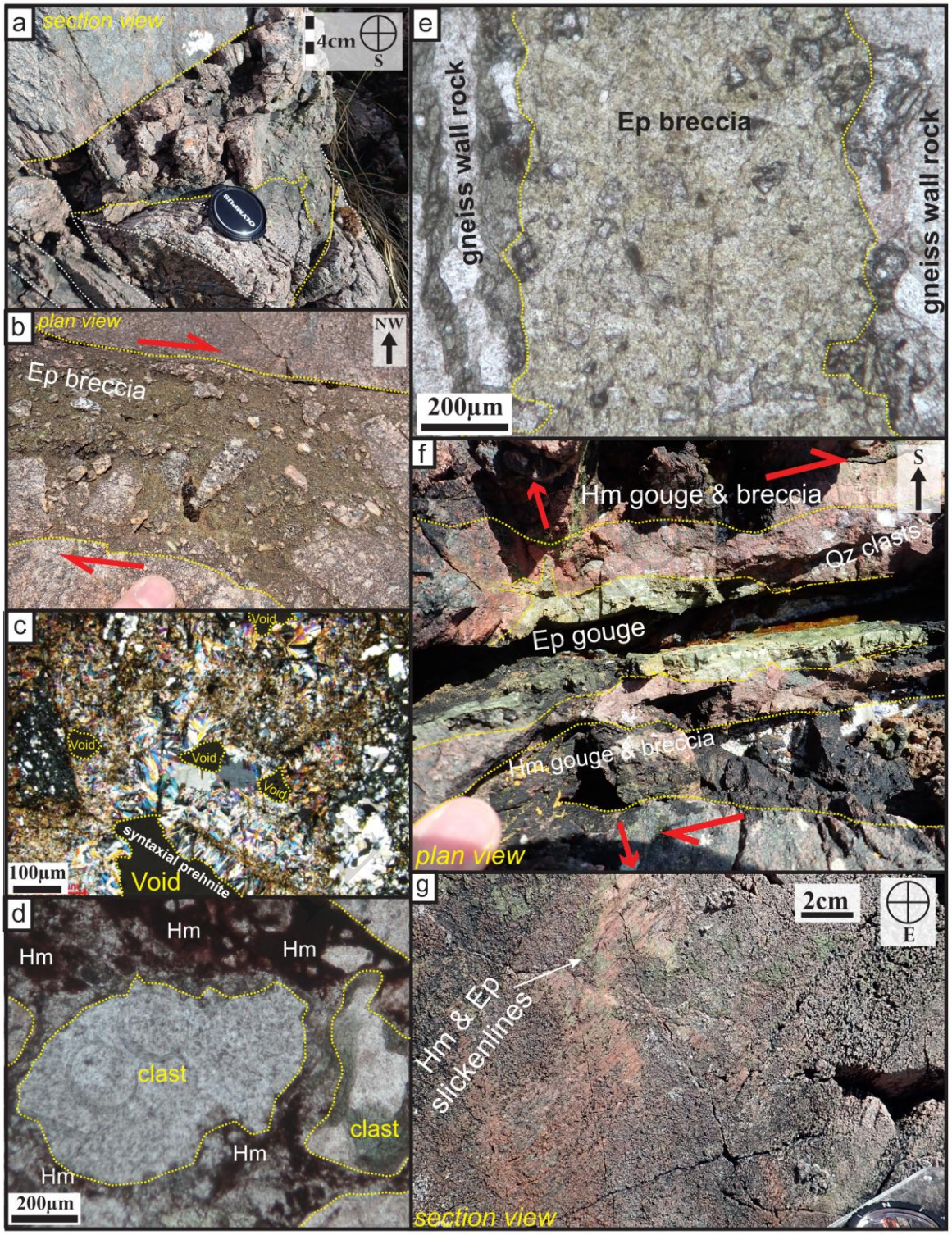

Figure 9

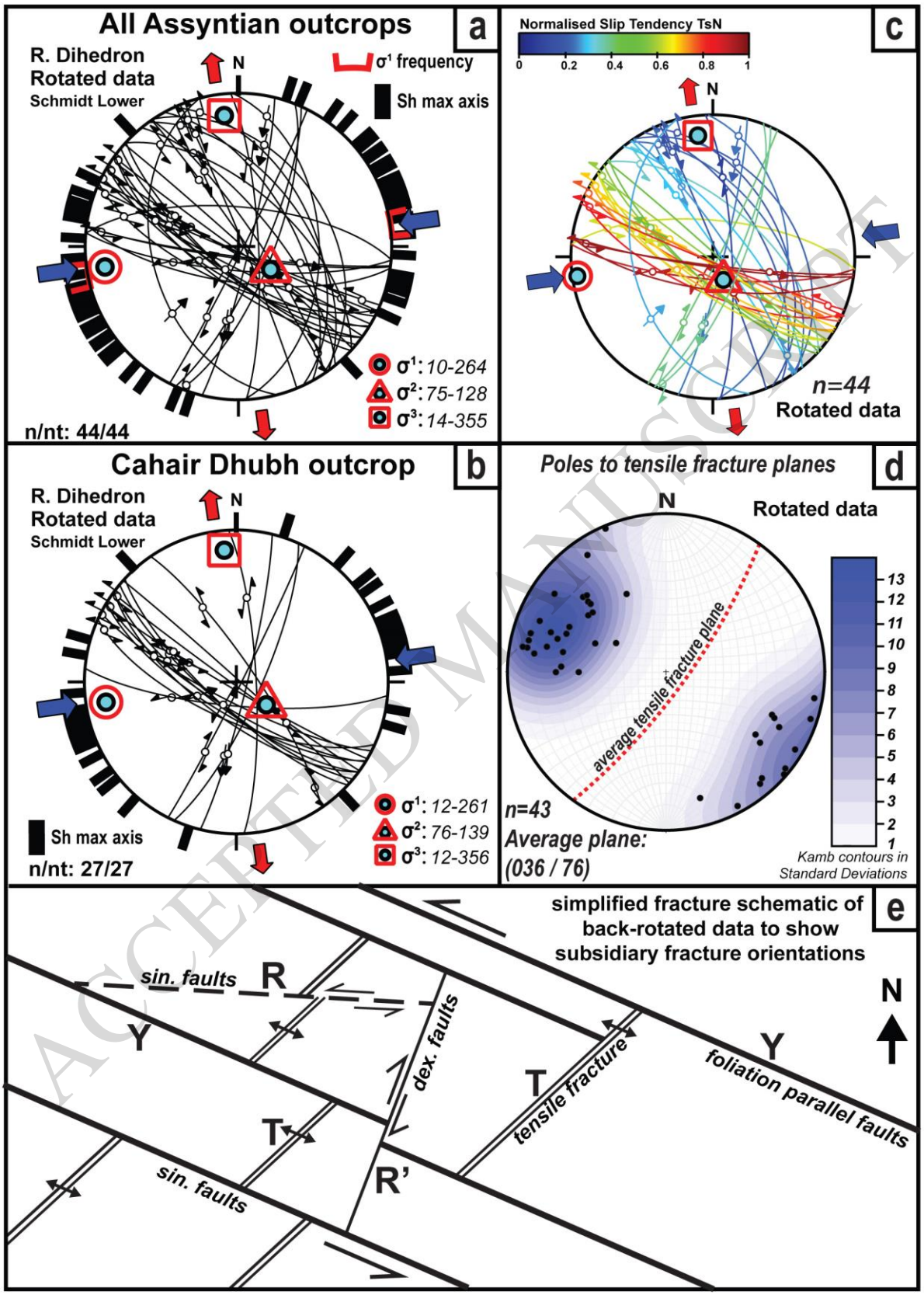

Figure 10

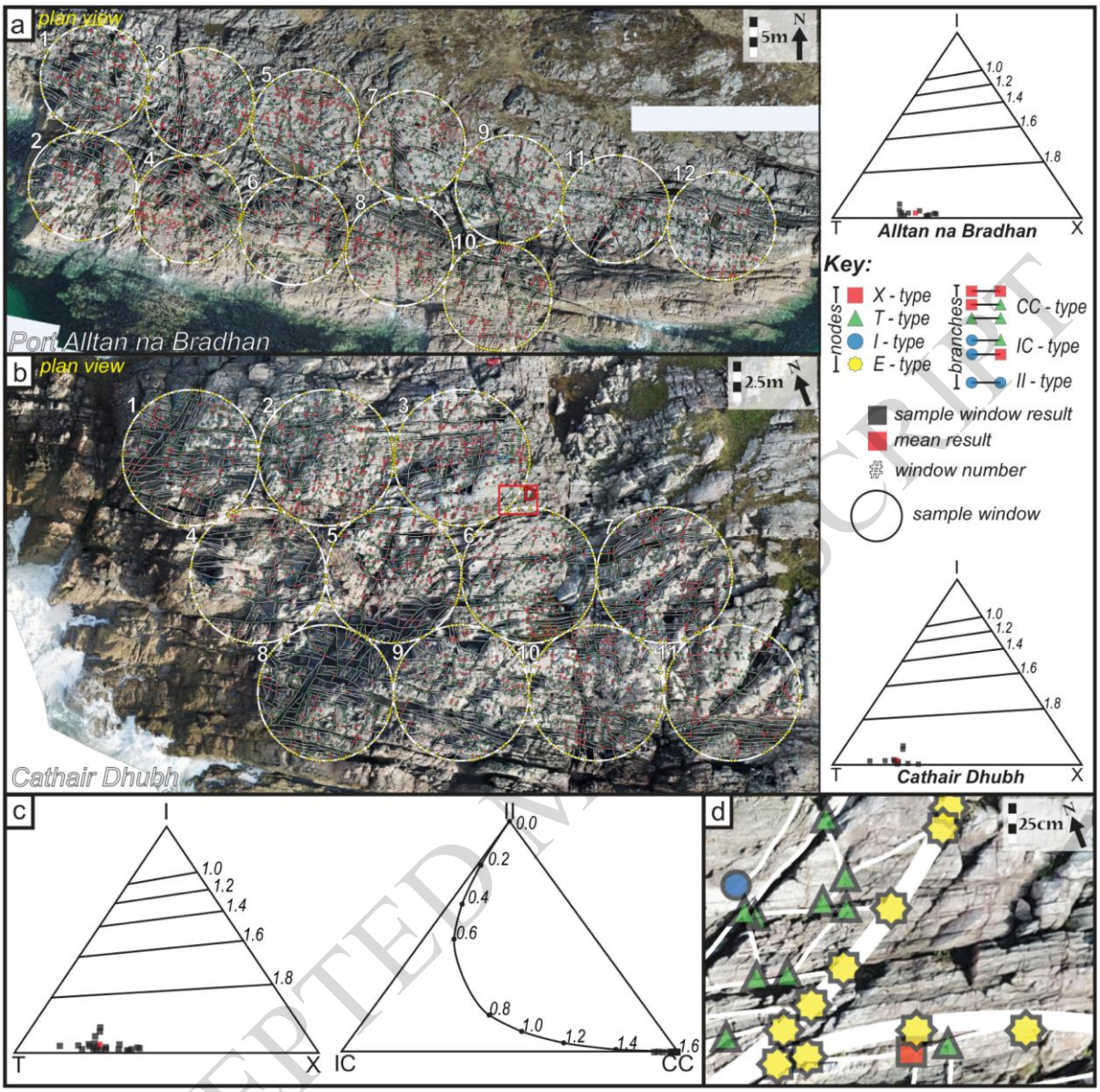

Figure 11

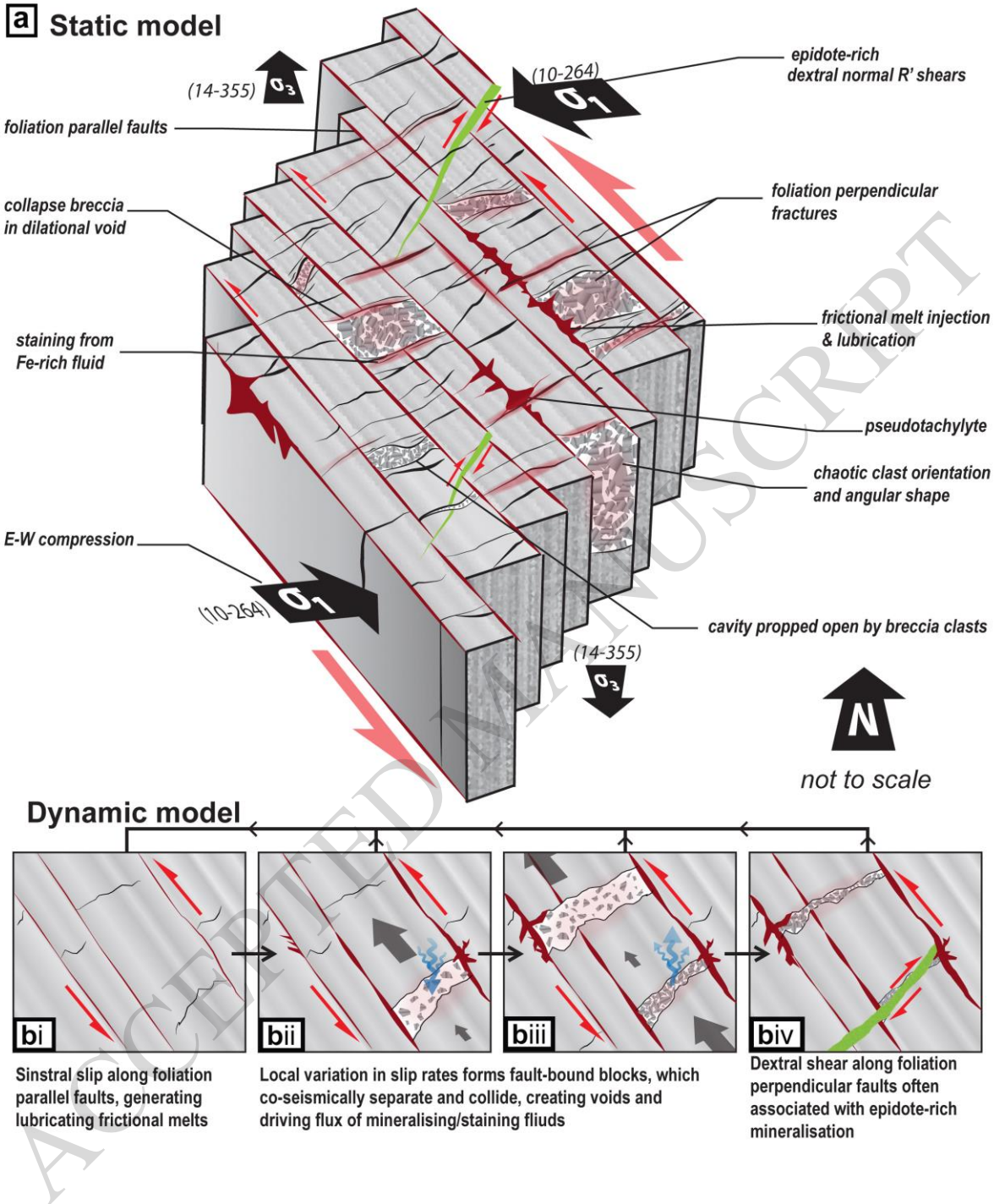

Sample	Cl	Cb	Node types - %			Branch types - %		
			I	T	X	II	IC	CC
CD_1	4.000	1.941	9	67	24	0.2	5.9	94.0
CD_2	4.448	1.984	3	74	24	0.0	1.6	98.4
CD_3	4.778	1.994	1	65	34	0.0	0.6	99.4
CD_4	3.551	1.929	11	66	23	0.0	7.1	92.9
CD_5	4.457	1.994	1	73	26	0.0	0.6	99.4
CD_6	4.225	1.979	3	74	23	0.0	2.1	97.9
CD_7	4.587	1.992	1	69	30	0.0	0.8	99.2
CD_8	3.764	1.983	3	84	14	0.0	1.7	98.3
CD_9	3.950	1.982	3	77	20	0.0	1.8	98.2
CD_10	4.365	1.986	2	72	25	0.0	1.4	98.6
CD_11	4.282	1.993	1	77	22	0.0	0.7	99.3
CD_Mean	***4.219***	***1.978***	***3***	***73***	***24***	***0.0***	***2.2***	***97.8***
AnB_1	4.521	1.980	3	64	33	0.0	2.0	98.0
AnB_2	3.971	1.956	7	70	23	0.0	4.4	95.6
AnB_3	4.811	1.993	1	61	38	0.0	0.7	99.3
AnB_4	5.028	1.996	1	62	37	0.0	0.4	99.6
AnB_5	5.145	1.991	2	58	41	0.0	0.9	99.1
AnB_6	4.670	1.997	0	62	37	0.0	0.3	99.7
AnB_7	4.364	1.996	1	73	27	0.0	0.4	99.6
AnB_8	4.912	1.989	2	58	40	0.0	1.1	98.9
AnB_9	4.294	1.985	2	71	26	0.0	1.5	98.5
AnB_10	4.202	1.996	1	71	28	0.0	0.4	99.6
AnB_11	4.174	1.987	2	69	29	0.0	1.3	98.7
AnB_12	3.943	1.976	4	71	25	0.0	2.4	97.6
AnB_Mean	***4.503***	***1.987***	***2***	***66***	***32***	***0.0***	***1.3***	***98.7***
Total Mean	**4.367**	**1.983**	**3**	**69**	**28**	**0.0**	**1.7**	**98.3**

Table I) Table summarizing the results of topological analysis from the Cathair Dhubh (CD) and Alltan na Bradhan (AnB).